Radiation Measurements 174 (2024) 107125

Contents lists available at ScienceDirect

Radiation Measurements

journal homepage: www.elsevier.com/locate/radmeas

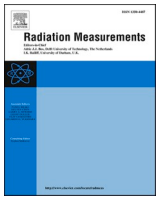

Radioluminescence-based fibre-optic dosimeters in radiotherapy: a review

Ivan Veronese [a,*], Claus E. Andersen [b], Enbang Li [c], Levi Madden [d], Alexandre M.C. Santos [e,f,g]

[a] Department of Physics, University of Milan and National Institute for Nuclear Physics, Milano Unit, Italy
[b] Department of Health Technology, Technical University of Denmark, Denmark
[c] School of Physics, Faculty of Engineering and Information Sciences, University of Wollongong, Australia
[d] Northern Sydney Cancer Centre, Royal North Shore Hospital, Australia
[e] Australian Bragg Centre for Proton Therapy and Research, Australia
[f] Radiation Oncology, Central Adelaide Local Heath Network, Australia
[g] School of Physics, Chemistry and Earth Sciences, The University of Adelaide, Australia

ARTICLE INFO

Keywords:
Dosimetry
PSD
Optical fibre
Scintillation
Radioluminescence
Radiotherapy

ABSTRACT

Since their conception in the early 1990s, radioluminescence-based fibre-optic dosimeters (FODs) have attracted great interest for dosimetric applications in radiotherapy (RT). Over the years, many scintillating materials, both organic and inorganic, have been developed and tested by multiple research groups around the world. In parallel, reliable techniques for removing or subtracting the stem effect, one of the main drawbacks of FODs, have been proposed in the literature. To date, several prototype systems are widespread, some of which prove to be viable commercial solutions. This review aims to trace the efforts over the years that have enabled FODs to become reliable tools for dosimetry in the current RT procedures and promising options for future scenarios. After a first section devoted to a thorough discussion of the stem effect issue, the use of FODs in various applications of interest to RT, primarily small-field dosimetry and *in vivo* dosimetry, are addressed. Their use both in external beam RT, including hadrontherapy, and in brachytherapy are considered. A special focus is given to the peculiarities of MRI LINAC dosimetry and the contributions of FODs in this context. Finally, the state of the art concerning the development and characterization of FODs for monitoring ultra-high dose rate radiation beams, typical of FLASH therapy and microbeam RT are presented, highlighting the challenges still open.

1. Introduction

Fibre-Optic Dosimeters (FODs) can be generally defined as a class of dosimeters using optical fibres as the signal transmission media, the sensing parts can be any materials which are sensitive to ionizing radiation. Different types of FODs have been developed and extensively investigated. These include, for example, those based on Optically Stimulated Luminescence (OSL), radiophotoluminescence (RPL), Cerenkov light detection, and fibre Bragg gratings-based sensors. Details of these systems and their applications can be found in several research papers and reviews, for instance in O'Keeffe et al. (2008), Yukihara and McKeever (2008), McKeever et al. (2020), Won Jang et al. (2012), Lebel-Cormier et al. (2021), Zhang et al. (2022). This review is on the most recent research and developments of radioluminescence-based FODs and their applications in medical radiotherapy (RT). This class of detectors exploits the principle of radioluminescence (RL) as a real-time indicator of the dose rate absorbed by the scintillating material. The radioluminescence material used by these types of FODs can be either a small piece of plastic scintillator, a single crystal of inorganic scintillator, a polymer dispersion containing the scintillating material in form of powder, or a piece of scintillating optical fibre, which can be made either of an organic or inorganic scintillating material. When plastic scintillating materials are used as the sensing elements in FODs, they become "plastic scintillation detectors" (PSDs) as are known in the literature. In is worth noting that such acronym uses the generic term "detector" to emphasise the fact that these systems can be used not only for dose measurements, but also for other detection applications, including counting and spectral measurements, when coupled with suitable photodetectors. In fact, at the end of the optical fibre is an optical detector, generally consisting of either a photomultiplier tube (PMT), photodiode, CCD camera, or spectrometer.

FODs offer several unique advantages for dosimetry in medical RT, including water/tissue equivalency for PSDs, compact sensitive volume, high sensitivity, real-time monitoring, and the absence of electrical

* Corresponding author. Department of Physics, University of Milan, and National Institute for Nuclear Physics, Milano Unit Via Celoria 16, 20133, Milano, Italy.
E-mail address: ivan.veronese@unimi.it (I. Veronese).

https://doi.org/10.1016/j.radmeas.2024.107125
Received 6 February 2024; Received in revised form 25 March 2024; Accepted 12 April 2024
Available online 15 April 2024

interference. These features of FODs make them extremely attractive for the dosimetry in the well-developed radiotherapies such as X-ray/gamma-ray based external beam RT, as well as in other RT modalities such as brachytherapy and hadrontherapy. FODs also play more and more important roles in developing novel RT modalities, such as MRI-LINAC treatments, Microbeam RT (MRT) and FLASH RT.

The potential applications of FODs have stimulated a wide range of research interests in multiple areas including material science, design and fabrication of various probes, novel techniques for stem effect removal, and signal processing methodologies and algorithms. A large number of research results and publications, therefore, have been generated in the topic of FOD.

Regarding the specific applications of FODs in RT, a bibliography search performed during the first week of December 2023 in "All Databases" and "Collections" of the Web of Science platform, using the appropriate Boolean combinations of the terms "optical fibre", "dosimetry", and "radiotherapy" (including their variants and synonyms) as keywords in the field "Topic", returned a total of 594 records published between 1983 and 2023. Approximately 50% of these records were published in the last 10 years and have been cited more than 2000 times.

332 of the 594 records also contained the term "radioluminescence" or "scintillation" (or their various variants) in the "Topic" field. Of these 332 records, 32 relate to publications on Radiation Measurements journal and 80 are published in journals more specifically oriented towards medical physics topics such as Medical Physics (42), Physics in Medicine and Biology (34) and Physica Medica- European Journal of Medical Physics (4). Of the 332 records mentioned above, 240 are classified as "article/research article" (190) or "proceedings" (50) published in peer review journals; 69 are "proceedings" published in indexed journals devoted solely to contributions at congresses and conferences; 6 are reviews and the remaining records are related to "dissertation/thesis" and 'patent'.

The review articles already available in the literature present different aspects of the research and development as well as applications of FODs. One of the most recent reviews on FODs is a general review of fundamentals and applications not only in RT, but also in other areas such as nuclear reactor physics as well as various tests and experiments with severe radiation conditions (Watanabe, 2023). Another review paper by Zhang et al. (2022) presents the current development of optical fibre-based radiation sensors, focusing on relevant advanced fibre materials and structures, fabrication methods of intrinsic all-fibre radiation sensors, and applicable scenarios from medical dosimetry to industrial environmental monitoring. A review on FOD applications in the emerging MRI-LINAC treatments was published by Madden et al. (2022). In 2020, Ding et al. published a review paper specialising on the development of inorganic scintillator-based fibre dosimeters for medical radiotherapy dosimetry, particularly focusing on real-time *in vivo* dosimetry (Ding et al., 2020). Other reviews on FODs available in the literature and published before 2020 include (Archer and Li, 2018) and the paper by Woulfe et al. (2016) about the role of FODs in in-vivo dosimetry for prostate cancer radiotherapy. In addition, it is noteworthy to highlight the book edited by Beddar and Beaulieu (2016), entirely focused on scintillation dosimetry and the related clinical applications.

This review aims to trace the efforts over the years that have enabled FODs to become reliable tools for dosimetry in the current RT procedures, and promising options for future radiotherapy scenarios. A first section of this article is therefore devoted to the so called "stem effect" that has been a major limitation to the use of FODs in clinical dosimetry for RT for several years. In addition to the solutions proposed to address the stem effect issue, the scintillating materials used to manufacture the mainly investigated FODs are accordingly referred. Afterwards, the use of FODs in various applications of interest to RT, primarily small-field dosimetry and *in vivo* dosimetry, are addressed. Their use both in external beam RT, including hadrontherapy, and in brachytherapy are considered. A special focus is devoted to describing the contribution that PSDs have made, and can make, in the context of dosimetry in the presence of magnetic fields, primarily in MRI-LINAC machines. Finally, the state of the art concerning the development and characterization of FODs in the context of monitoring ultra-high dose rate radiation beams, typical of FLASH therapy and microbeam RT are presented, highlighting the challenges still open.

2. Stem effect

2.1. Components of the stem effect and detection methods

The stem effect is a phenomenon encountered by several real-time dosimeters that require signal carriers to transport dose-response signals from sensitive volumes to a readout system. When irradiated, the signal carrier can produce a measurable signal that offsets the dose-response signal generated by the dosimeter's sensitive volume (Marckmann et al., 2006). For charge collecting dosimeters, the stem effect can occur when transmission cables are irradiated, though these perturbations are typically small. However, in the case of FODs, the irradiation of their optical fibres can seriously compromise the accuracy of their dose measurements.

In general, most of the literature describing the stem effect in FODs and the solutions adopted for its correction or removal attributes the origin of the stem effect to two phenomena: Cerenkov radiation and fluorescence. The term fluorescence is often used in a very general conception as it can encompass many phenomena caused by different physics. In fact, fluorescence may be due to the intrinsic scintillation properties of the material constituting the optical fibre and therefore the physical processes will be different according to the composition of the light guide, i.e. typically silica or polymethyl methacrylate (PMMA). In addition, phosphorescence may occur as a consequence of charge trapping and de-trapping phenomena at room temperature, with intrinsic defects acting as shallow traps in fibre material (Veronese et al., 2007, 2015).

Another phenomenon that contributes to stem signals in optical fibres is Cerenkov radiation (Jelley, 1955). Cerenkov radiation is generated in a dielectric medium when a charged particle with a velocity greater than that of light in the medium is passing through the medium. The characteristic lifetime for Cerenkov radiation lies in the picosecond range. The threshold kinetic energy T for Cerenkov radiation produced by an electron passing through the medium with velocity v is equal to:

$$T = \frac{m_0 c^2}{\sqrt{1-\beta^2}} - m_0 c^2 \tag{1}$$

where $m_0 c^2$ is the rest energy of the electron (i.e. 511 keV); $\beta = \frac{v}{c}$ is the ratio of the electron velocity v to the speed of light in vacuum c. The values of threshold energy in media like silica and PMMA, (refractive index n of 1.46 and 1.49), are equal to approximately 190 keV and 178 keV, respectively. Such energies are significantly lower than the energy of electron beams used in external RT, as well as of those of secondary electrons originated by the interaction of megavoltage X-rays produced by medical linear accelerators.

The Cerenkov emission spectrum is continuous with spectral distribution proportional to $1/\lambda^2$. Photons are emitted anisotropically following a cone-shaped distribution aligned with the direction of the travelling particle. The angle θ of the Cerenkov cone is directly related to the velocity of the charged particle, according to:

$$cos\ \vartheta = \frac{1}{n \bullet \beta} \tag{2}$$

The proportion of fluorescence, phosphorescence and Cerenkov light induced in the optical fibre can be different depending on the fibre materials and the radiation conditions. It is possible to identify the main contributions of the stem effect through appropriate investigations. In particular, changes in the angle of incidence of the ionizing radiation on

the optical fibre and the use of radiation beams of different qualities make it possible to assess the extent of the Cerenkov contribution with respect to fluorescence, especially if accompanied by wavelength-resolved measurements. Time-resolved measurements of the light output, on the other hand, allow the extent of phosphorescence phenomena to be assessed in comparison with the more rapid fluorescence and emission of Cerenkov light. Some examples of the application of such approaches are summarised below.

A method often used to check for the presence of Cerenkov radiation consists of exploiting the angle dependence of the Cerenkov light by irradiating the optical fibre with electron beams of a few MeV produced by a LINAC, varying the angle of incidence between the beam and the axis of the optical fibre. Such approach was firstly used by (Beddar et al., 1992a) who demonstrated that the mechanism by which light was induced in optical fibres and other light pipes (PMMA, polystyrene and water) when exposed to radiotherapy electron beams was the Cerenkov radiation. They did not find evidence for significant amounts of light generated by other mechanisms.

Analogous investigations were performed by de Boer et al. (1993) using hard-core silica fibres acting as lightguide for different types of plastic scintillators. They observed the expected angle dependence of the Cerenkov light. However, the results of wavelength-resolved measurements of the light emitted by the optical fibres irradiated with X-rays generated by an orthovoltage unit (i.e. below the Cerenkov energy threshold) led the authors to conclude that fluorescence was also a dominant source of fibre light.

Similar conclusions were drawn by Therriault-Proulx et al. (2013) after spectrometry studies performed during the irradiation of a PMMA bare optical fibre with ionizing radiation of different qualities (kilovolt X-rays from a superficial therapy unit, an ^{192}Ir high-dose-rate (HDR) brachytherapy source, a ^{60}Co source from an external-therapy unit, and megavoltage electron and photon beams from a linear accelerator). The authors showed that the stem effect can be expressed as a linear combination of Cerenkov light and fluorescence. The proportion of fluorescence and Cerenkov light induced in the fibre decreased as the irradiation energy increased. However, the fluorescence was present over the entire range of clinically relevant irradiation energies, including megavoltage energies.

Wavelength-resolved measurements of the stem effect in silica optical fibres were also performed by Veronese et al. (2013a, 2013b), focusing on the radioluminescence signal produced by Eu- and Ce-doped silica optical fibres irradiated with both soft X-rays and with megavoltage photon and electron beams produced by medical linear accelerators. The RL spectra obtained in different irradiation geometries in terms of portion of optical fibre exposed to the radiation and of beam orientations, led the authors to conclude that below the Cerenkov radiation energy threshold, a slight contribution to the total RL signal due to fluorescence effects occurred in the silica optical fibre. Above the energy threshold, the stem effect was mainly caused by Cerenkov radiation.

The components of the stem effect generated in Al_2O_3:C based FODs dosemeters were analysed by Marckmann et al. (2006) to determine their impact on the RL signal. Both silica and PMMA fibres were considered, exposed to radiation beams of different qualities. Temporal measurements performed using 12 MeV electrons and 6 MV photon beams indicated that phosphorescence was not the mechanism causing the observed stem effect. Furthermore, the results from spectral measurements obtained by irradiating the FODs with a ^{90}Sr/^{90}Y beta source and with soft X-rays showed that, for the investigated fibres, the stem effect was mainly caused by fluorescence and that it was equally generated in PMMA and silica fibres. No significant angle dependence of the stem effect on the incident angle of radiation was observed when 6 MeV electron beams were used, indicating that Cerenkov radiation was not the main contributor.

Table 1 summarizes the main components of the stem effect in RL-based FODs and the methods for their detection and discrimination.

Table 1
Components of the stem effect in FODs and methods used for their detection and discrimination.

Stem effect component	Methods of detection
Cerenkov light	- Check of the angle dependence of the light intensity under irradiation with electron beams above the Cerenkov threshold energy - Spectral measurements
Fluorescence	- Measurement using ionizing radiation below the Cerenkov threshold energy - Spectral measurements
Phosphorescence	- Time-resolved measurements

2.2. Methods for stem effect correction

Several approaches have been implemented to account for the stem effect signal generated in FODs. An overview of the main methods described in the literature is given below.

2.2.1. Twin-fibres

The twin-fibres approach was first proposed by Beddar et al. (1992b, 1992c, 2007) who developed a detector consisting of a plastic scintillator embedded in a small polystyrene probe and optically coupled to an optical fibre light guide. A second identical parallel fibre light guide which was not connected to the scintillator was used for subtraction of the stem effect. A sketch this PSD is shown in Fig. 1.

Afterwards, the twin-fibre method was employed by various authors using different types of scintillators and optical fibres (Létourneau et al., 1999; Yoo et al., 2013; Carrara et al., 2014; Debnath et al., 2021). This approach gave reliable results in various studies performed under controlled irradiation scenarios, e.g. use of large radiation fields with a fixed collimator and gantry angle. However, the twin fibre method showed some weaknesses in more complex irradiations, typical of the modern external radiation treatment modalities. Indeed, in these conditions the amount of stem effect generated in the two paired fibres has shown to be different (Liu et al., 2011).

Liu et al. (2013) attributed these differences to a combination of four geometric factors: (1) the different amount of scattered radiation at the location of the two fibres; (2) the fact that at certain beam angles one fibre is closer to the radiation source than its partner; (3) one fibre shields its partner from low energy scattered electrons; and (4) one fibre acts as buildup material for the partner fibre. To overcome these limitations, the use of a twisted pair of optical fibres was proposed. The twisted pair consisted of a fibre carrying the scintillation signal that was twisted with a second optical fibre to form a double helix. In this geometry, both the signal fibre and the background fibre experience, on average, the same radiation environment, independently of the irradiation scenarios. This method was used by Liu et al. (2013) for subtracting the residual stem effect occurring in an air core dosimeter system (Lambert et al., 2008, 2010; Liu et al., 2011).

2.2.2. Optical filtering

The optical filtering method attempts to separate the scintillation signal from the stem effect exploiting their different spectral emission, by means of an optical filter or a suitable combination of multiple optical filters. Since the emission of Cerenkov light, although spanning the entire visible spectrum, has an intensity that decreases as the wavelength increases, the optical filtering approach is more efficient for long-wavelength scintillators, i.e. scintillators with emission occurring in the red or infrared spectral region.

One of the earliest studies where optical filtering was employed to face the drawback of the stem effect in FODs was conducted by de Boer et al. (1993). Various plastic scintillators were considered. Some of them are commercially available and others were specially developed in combination with various long-pass filters. The results showed how the

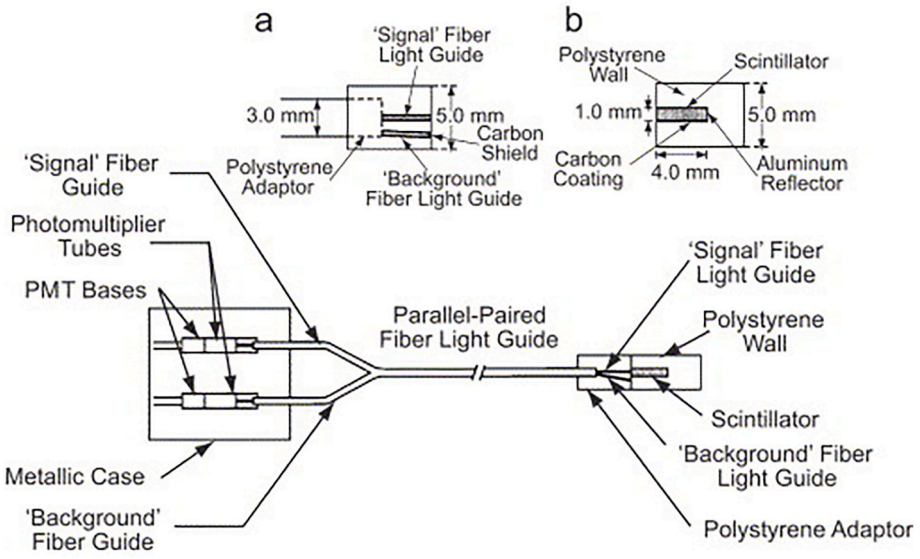

Fig. 1. Diagram of the first PSD exploiting the twin-fibres approach for stem effect correction, together with details of the longitudinal cross-sections of (a) the proximal end of the fibre light guide and (b) the polystyrene probe containing the scintillator. (Reproduced from Beddar, 2007).

optical filtering approach, although not resolutive, allowed a significant reduction in the stem effect contribution. A point highlighted in the study concerned the limited number of efficient long-wavelength scintillators available and the need to focus the research on the development of new and more efficient ones.

In fact, significant progress has been made since de Boer's research (De Boer et al., 1993), and numerous studies report on the performance of long-wavelength scintillators where the optical filtering method is applied for the removal, or reduction, of the stem effect. Some examples, relating to both organic and inorganic scintillators, are given below. Clift et al. (2000) using a BC-430 plastic scintillator characterised by a RL emission centred at 580 nm, together with a combination of optical filters in front of the photodetector, achieved a contribution of the Cerenkov and fluorescence signal to the scintillator probe output equal to approximately 3% under the experimental conditions employed. Lee et al. (2007) using 6 MeV and 12 MeV electron beams with different orientations, tested the efficiency of the optical filtering approach on a BCF-60 plastic scintillator, characterised by an emission centred at 530 nm. The greatest reduction of stem effect, in terms of independence of the luminescence signal of the beam angle, was achieved by interposing a combination of a 500 nm long-pass filter and a 480–600 nm band-pass filter between the light guide and the photodiode.

Concerning inorganic scintillators, Santiago et al. (2009) performed tests with Mn-doped Lithium Tetraborate, characterised by an RL emission centred at 600 nm, using a Co-60 as radiation source. A 530 nm long-pass optical filter was used to limit the stem effect in the characterization measurements of the implemented FOD.

Molina et al. (2012, 2013) investigated the RL properties of three red-emitting phosphor samples, i.e. $Y_2O_2S:Eu^{3+}$, $YVO_4:Eu^{3+}$ and $Y_2O_3:Eu^{3+}$, in view of FODs construction. In particular, the red emission near 625 nm from $Y_2O_2S:Eu^{3+}$ samples promoted a reduction in the stem effect by using a 610 nm long-pass filter in front of the PMT, during irradiation with a ^{60}Co source. The possibility to exploit the red RL emissions of Eu^{3+} to separate the scintillation signal from the spurious ones was also investigated by Veronese et al. (2013a, 2013b) through spectral analyses of the luminescence signal originated in Eu-doped silica FODs irradiated with photon and electron beams of different energies, field sizes and orientations. Fig. 2 shows examples of such spectra that clearly highlight how the change of the irradiation conditions may strongly influence the relative contribution of the stem effect over the Eu^{3+} RL signal, mainly because of the Cerenkov radiation.

Ramírez et al. (2016) applied the optical filtering method for studying the performance of a ZnSe(Te)-based FOD irradiated with electrons and photons originating from various radiation sources. The scintillator was characterised by a RL emission peaked at 626 nm. The percentage stem effect contribution per unit length remaining after using a 610 nm long-pass filter amounted to 0.24 %/cm in the applied experimental conditions. Another long-wavelength scintillating material exploited for FODs manufactory was ruby, i.e. Al_2O_3 doped with Cr^{3+} ions (Jordan, 1996; Teichmann et al., 2013). The RL emission peaked at 694 nm allows the use of a narrow band-pass filter to reduce the stem effect to negligible levels, in case of irradiation with a ^{192}Ir brachytherapy source (Kertzscher and Beddar, 2016).

A significant improvement in the efficiency of the optical filtering method can be achieved by using FODs manufactured using scintillators characterised by an infrared emission. This aspect was pointed out by Veronese et al. (2014, 2017) who demonstrated that the use of a 950 nm long-pass filter was sufficient to suppress the stem effect originated in Yb-doped silica based FODs irradiated with typical external RT beams, while preserving the Yb^{3+}emission centred at 975 nm. A similar approach was adopted by Kim et al. (2020) using Lanthanide-based rare-earth $NaYF_4$ nano-phosphors doped with both erbium and cerium as infrared scintillating material. The RL emission, peaked at 1550 nm, was separated from the stem effect contribution occurring at shorter wavelengths by means of a 1400 nm long-pass filter.

2.2.3. *Spectral discrimination and hyperspectral approach*

Similar to optical filtering, the spectral discrimination approach exploits the different spectra of scintillation and stem emissions. The mixed scintillation-stem signal of the FOD is measured in two different spectral regions, within the emission spectra of the scintillator, to extract only the signal that is proportional to the dose deposited in the scintillation probe. This approach assumes that the light signal produced by the FOD is a superposition of two spectra: Cerenkov light and scintillation signal (Archambault et al., 2012; Simiele and DeWerd, 2018). A direct correlation between the total light signal and the radiation dose absorbed by the FOD can be achieved by a suitable detection and analysis of such signal. Indeed, by splitting the light output in two channels (*1* and *2*), characterised by different wavelength filters, the dose absorbed by the FOD can be calculated as:

$$D = A \bullet M_{channel\ 1} + B \bullet M_{channel\ 2}$$

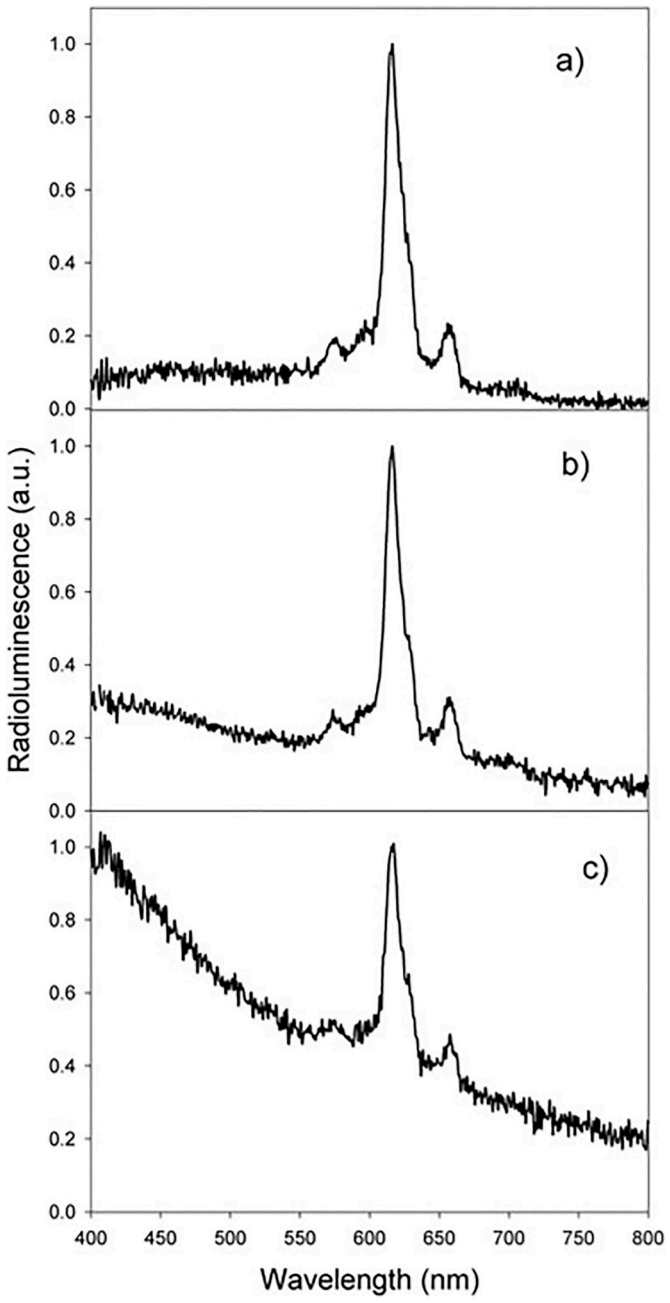

Fig. 2. RL spectra of the Eu doped silica optical fibre irradiated under different experimental conditions: small (a) and large (b) 6 MV X-rays field orthogonally impinging the FOD; 6 MV electron beam (c) impinging the FOD at angle of 45° relative to the fibre axis. (Reproduced from Veronese et al., 2013b).

where $M_{channel\ 1}$ and $M_{channel\ 2}$ are the light measurements obtained in the two channels and A and B are the calibration coefficients. The calibration coefficients are derived by irradiating the FOD in two different geometries so as to obtain two different ratios of scintillation signal to stem effect. From the ratio of the calibration coefficients, the so-called "Cerenkov light ratio" (CLR) can be derived (Guillot et al., 2011).

The spectral discrimination method for stem effect correction was first proposed by Fontbonne et al. (2002) by using a BCF-60 scintillator based FOD whose light output was detected by means of pin photodiodes covered by interference filters. Afterwards, the efficacy of this approach was tested by Frelin et al. (2005) and by Archambault et al. (2006) using a CCD as photodetector.

Guillot et al. (2011) demonstrated that the accuracy of the spectral discrimination method depends on the calibration procedure used to determine the calibration factors and on the attenuation properties of the optical fibre used. They tested different calibration procedures and identified the one that produced the measurements that were the least influenced by the length of optical fibre irradiated and the amount of Cerenkov light produced in the FOD. This procedure, based on the irradiation of two fibre portions of known length, was then recommended by the manufacturer of the commercial PSD systems Exradin W1 and W2 (Standard Imaging, USA), which also provides a dedicated solid water phantom and a plastic holder for the water phantom to be used for the calibration of these PSDs in a geometry involving radiation beams orthogonal to the fibre axis (Carrasco et al., 2015; Okamura et al., 2022).

When a FOD is oriented parallel to the beam axis alternative procedures are required (Morin et al., 2013; Underwood et al., 2015). In fact, the results of measurements of the stem effect as functions of depth and fibre beam angle performed with various light guides by Simiele and DeWerd (2018) highlighted the importance of characterizing the stem-effect, as small changes in the spectrum of the stem-effect can cause changes in the calibration factors.

The spectral discrimination method, originally developed for PSDs exposed to external radiation beams, was also tested in irradiation scenarios typical of brachytherapy treatments. Kertzscher et al. (2011) demonstrated through an in-phantom study that the spectral discrimination approach was suitable for Al_2O_3:C based FOD exposed to a 37 GBq ^{192}Ir source. An equivalent radiation source was employed by Ishikawa et al. (2015) to implement the spectral discrimination technique for a BC-490 PSD.

The spectral discrimination approach breaks down when more than two wavelength spectra are superposed. In order to overcome this limitation and pave the way to the development of multipoint FODs coupled to a single collection optical fibre, Archambault et al. (2012) proposed an extension of the mathematical formalism of the spectral discrimination method, by introducing a hyperspectral approach. Such approach was implemented by Therriault-Proulx et al. (2012) who developed a 2-point and a 3-point PSDs consisting of different scintillating elements (BCF-10, BCF-12 and BCF-60). The multi-point PSD HS-RP-200, currently marketed for research purposes by Medscint (Canada) applies the hyperspectral approach for its stem effect correction.

2.2.4. Time discrimination

Time discrimination methods exploit differences between the rise and decay constants of luminescence signals (e.g. scintillation) and stem signals. Many proposed temporal methods require pulsed radiation sources for such temporal discrimination of stem signals and luminescence signals of interest. To effectively discriminate between luminescence and stem signals, the decay constants of luminescence signals must be significantly different from the decay constants of stem signals.

The characteristic lifetime for Cerenkov radiation lies in the picosecond range while fluorescence occurring in typical optical fibres are characterised by lifetimes of few microseconds or less (Andersen et al., 2011; Beierholm et al., 2011; Martinez et al., 2015). No significant phosphorescence phenomena characterised by longer decay times have been reported for these typical optical fibres in the literature. Considering that for most medical LINACs, their pulse widths are a few microseconds in duration, and that the time interval between pulses is of the order of a few milliseconds, it is not particularly difficult to find inorganic scintillators with RL lifetimes compatible with the requirements time discrimination methods.

In fact, there are many studies in the literature concerning the characterisation of inorganic scintillators-based FODs in pulsed irradiation regimes, that make use of gating techniques to ensure scintillation light measurements only within suitable time-windows (i.e. blocking counting during and immediately after every beam pulse). Gating can be directly triggered by the synchronisation signal of LINACs, or by detecting ambient scattered radiation in the irradiation room, next to

the LINAC, using a scattered-photon trigger detector, usually still consisting of a scintillator coupled to an optical fibre (Tanyi et al., 2010; Magne et al., 2013).

Jordan (1996) carried out measurements with a ruby crystal. The ^2E-$^4A_2$ transition of Cr in ruby at 694 nm has a lifetime of approximately 3 ms, much longer than the lifetime of the stem effect. The author achieved an effective elimination of the stem effect by combining optical filtering and time-delayed gated signal measurements. A ruby-based FOD was also investigated by Teichmann et al. (2013) by applying the time gating method to deal with the stem effect. Justus et al. (2006) and Tanyi et al. (2010, 2011) applied the time gating method to study the performance of a Cu^+-doped quartz based FOD, whose scintillation signal was characterised by a bi-exponential decay curve with time constants of approximately 50 and 100 μs. The time gating approach was widely employed with Al_2O_3:C based FODs. Radioluminescence in Al_2O_3:C primarily originates from direct recombination through the F-centres. This process involves a ~35 ms relaxation time, i.e. much longer than the lifetime of the stem effect signal and suitable for time gating correction (Andersen et al., 2006, 2011; Beierholm et al., 2008, 2011; Magne et al., 2013). Martinez et al. (2015, 2017), characterised YVO:Eu-based FODs using the time gating method, exploiting the scintillation decay curve of YVO:Eu featuring two main decay components with time constants of approximately 12 μs and 0.5 ms. Similarly, Teichmann et al. (2017) tested the feasibility of stem-removal by gated detection of the RL signals of a BeO-based FOD. The RL lifetime of BeO was of approximately 27 μs at room temperature and a time stamp-based data acquisition and analysis, not needing for triggering, was employed.

Considering the advantages in terms of tissue-equivalence for plastic scintillators compared to the inorganic ones, the interest in the applicability of time discrimination methods for PSDs is high. However, this aspect is particularly challenging since ensuring sufficiently high signal-to-noise ratios proved difficult. This is mainly due to the short RL lifetime of PSDs, resulting in a large signal loss when applying classical temporal gating approaches. Beierholm et al. (2011) tested time discrimination methods with both a custom-made plastic scintillator and with the commercial one BCF-60. The former was characterised by a two-component scintillation signal decay curve with characteristic times of approximately 6 and 22 μs. For the latter, a scintillation time of the order of 13 μs was estimated. The results of the application of standard gating techniques demonstrated that, although this method seemed theoretically achievable, the signal-to-noise ratio and accuracy was not sufficient if the organic scintillator luminescent lifetime was not significantly different from the stem signal lifetime as well as from the LINAC pulse duration.

For PSDs, alternative time discrimination approaches based on a direct analysis of the voltage-time waveforms, measured with a sufficiently high temporal resolution during the irradiation, were proposed. Clift et al. (2002) tested a PSD manufactured using a commercial BC-444 scintillator having a long decay time of approximately 260 ns, using pulsed electron beams of width equal to 0.45 μs. The current output of the photodiode used to detect the PSD light signal, converted into a voltage and amplified, was measured with a 100 MHz digital oscilloscope. A Cerenkov and fluorescence radiation (CFR) detector was also used to measure the voltage waveform due to the stem effect only. The CFR detector design was identical to the PSD design, except that it had a section of light guide material in place of the scintillator. The results showed that CFR detector output finished at approximately 700 ns after the start of the irradiation pulse. A 5 ns sampling time in the interval 700–705 ns was used for the PSD waveform integration that enabled to remove almost completely the Cerenkov light, at the expense of 44% of the scintillation light, in the specific irradiation conditions applied. The conclusions highlighted that the development of longer decay constant plastic scintillators would ease the LINAC conditions required to implement a time discrimination approach.

Archer et al. (2017a, 2018b, 2019a) and Madden et al. (2018a, 2018b) developed signal modelling algorithms to avoid scintillation loss during the analysis of voltage-time waveforms. First, Archer et al. (2017a) proposed a derivative guided approach. Using the BC-444 PSD with a decay constant of 285 ns, it was demonstrated that 74% of the stem signal could be eliminated with only 1.5% loss in scintillation signal (Archer et al., 2017a). Further improvements in stem effect removal were made through analysis of the BC-444 scintillation signal's exponential rise and decay in the voltage waveform (Archer et al., 2018b). Theoretical modelling of the time-dependent scintillation signals and stem signals was proposed by Archer et al. (2019a), tested using the same setup as used in (Archer et al., 2018b). At the expense of 0% of the scintillation signal, Archer et al. (2019a) reported that average errors for beam profiles were within (1–3) % of reference ionization chambers. Madden (2022) generalised and refined the theoretical model published by Archer et al. (2019a). With the refined theoretical model, mean errors of beam profiles with respect to reference ionization chamber measurements were reported to be 0.7 % in central regions and 0.9 % in out-of-field regions of beam profiles; comparable to the performance of two fibre subtraction Madden (2022).

Analysis of voltage-time PSD waveforms using artificial intelligence approaches was proposed by Madden et al. (2018a, 2018b). Initially, shallow artificial neural networks were trained to estimate the stem effect component present in waveforms originated by the PSD (Madden et al., 2018a). Using the same BC-444 PSD as in (Archer et al., 2017a, 2018b, 2019a; Madden et al., 2018a), improved performances were achieved by using a convolutional neural network. When applied to unseen data, the deep-learning based analysis method was reported to have performed comparably to that of the twin-fibres approach (Madden et al., 2018b).

2.2.5. Air core light guide

All the methods described so far are based on the non-detection, or appropriate subtraction, of the signal contribution due to the stem effect. A different approach described in the literature consists instead of preventing the generation of the stem effect by using an air core light guide to transport the scintillation signal out of the primary radiation field. Indeed, in such case no Cerenkov light is produced because the refractive index of air is close to unity.

The use of an air core light guide was first proposed by Lambert et al. (2008). They constructed a BC-400 based PSD inserted into one end of an air core light guide in the form of a hollow silica tube coated inside with a thin layer of silver. Air core light guides of different lengths, equal to 20 cm, 60 cm and 100 cm were tested. The end of the light guide opposite the scintillator was coupled with a PMMA extension fibre used to transmit the scintillation light to a PMT located outside the radiotherapy bunker. The dosimetric performances of the FOD having a 20 cm long air core light guide were deeply investigated by Lambert et al. (2010) and compared with those of standard dosimeters.

Ralston et al. (2012) used an air core based FOD, in combination with radiochromic films, to derive diode correction factors for small radiotherapy fields.

Eichmann and Thomann (2017) considered the air core concept in FODs properly modified to meet the requirements of dosimetry in brachytherapy. In particular, air core light guides with length from 5 mm to 17 mm were manufactured in-house using mylar foils. The air core based FOD measured the dose rates from $^{106}Ru/^{106}Rh$ eye plaques with an uncertainty of the order of 5% without any form of correction for the stem effect.

In the case of irradiation of air core based FODs with external radiotherapy beams, energetic scattered radiation can still generate a residual stem effect signal in the optical fibre coupled with the air core light guide. The scattered radiation is not subject to the high dose gradients that exist within and at the edge of the primary radiation fields. Therefore, simple twin fibre methods for removing the residual stem effect proved to be sufficiently accurate (Lambert et al., 2010; Liu et al., 2013). Alternatively, an approach based on the use of remotely operated shutter to block the scintillation signal in order to determine the amount

of the residual stem effect induced in the extension fibre to be subtracted to the total luminescence signal was proposed (Lee et al., 2013).

2.2.6. Real-time OSL

For FODs using inorganic materials with OSL properties, in addition to the RL ones, a real-time OSL read-out method has been developed that avoids the measurement of stem signals. This method, termed the real-time OSL (rtOSL) technique, applies a pulsed optical stimulus during the irradiation of the inorganic material. During optical stimulation, measured signals are comprised of stem signals, RL and OSL; without stimulation, measured signals are comprised solely of stem signals and RL. Theoretically, the difference between signals with and without stimuli corresponds purely to OSL, free of stem and RL. This method was first proposed by Gaza et al. (2004, 2005) using an Al_2O_3:C single crystal based FOD and a Nd:YAG system with a medical LINAC. For the experimental setup used by Gaza et al. (2004) an accumulated-dose dependent rtOSL signal was reported. This behaviour was theoretically expected as trapping centres were not completely emptied by single pulses of optical stimulation (Polf et al., 2004). To correct this dependence, Gaza et al. (2004, 2005) proposed an iterative correction termed the ΔrtOSL correction. Using the ΔrtOSL correction, percent-depth-dose (PDD) curves measured using the rtOSL FOD were restored to within 2 % agreement of PDD curves measured by an electron diode.

Santos et al. (2019) investigated a BeO ceramic based FOD using the rtOSL method for superficial X-ray measurements, motivated by BeO's tissue equivalence across superficial energies. For this BeO FOD, ΔrtOSL corrected signals were reported to have uncertainties ranging from 10 to 15 % (Santos et al., 2019). The authors attributed these unacceptable uncertainties to result from poor signal-noise ratios of measured rtOSL signals, subsequently exacerbated by the ΔrtOSL correction. To address this challenge, Madden et al., (2020) applied temporal modelling theory and corrected fitted signals using an exponential based correction. Through the retrospective application of temporal modelling methods rtOSL signals recorded during the study of Santos et al. (2019) uncertainties were reported to decrease to (3.4–6.5) %. Finally, Madden et al. (2021a) proposed a deconvolution approach to the rtOSL accumulated-dose correction. An optimised BeO rtOSL FOD was employed for the measurement of dose rate dependences with a medical LINAC, and the performance of the deconvolution correction was benchmarked against the ΔrtOSL correction and the temporal modelling method. On average, the corrected rtOSL's dose uncertainties were reported to be 1.9 % for the deconvolution correction, 5.4 % for the temporal modelling correction and 6.4 % for the ΔrtOSL correction (Madden et al., 2021a).

For OSL materials with sufficiently fast decay-constants, the rtOSL accumulated-dose dependence can be avoided. In particular, KBr:Eu appeared particularly interesting for real-time OSL dosimetry. Indeed, along with the fast luminescence lifetime of the $4f^6 5d\text{-}4f^7$ transition in Eu^{2+} of the order of 1 μs (Sosa et al., 1995; McKeever 2011), a complete depletion of the KBr:Eu OSL signal can be achieved in tens of millisecond by means of a suitable red light stimulation (Klein and McKeever, 2008), making correction algorithms to account for undepleted OSL unnecessary. A first example of the use of such approach was reported by Gaza and McKeever (2006) who studied the rtOSL dose-rate dependence of KBr:Eu based FODs prepared with different Eu dopant concentration and irradiated with a $^{90}Sr/^{90}Y$ source. Afterwards, tests performed using various radiation sources of medical interest like an ^{192}Ir brachytherapy seed source, accelerated proton beams and computed tomography (CT) X-rays demonstrated the performance of the rtOSLapproach in KBr:Eu based FODs (Klein and McKeever 2008; Klein et al., 2010).

2.3. Comparison of the methods and summary remarks

Various studies in the literature show direct comparisons among different methods of correction for the stem effect in FODs.

Liu et al. (2011) studied the performances of three methods for dealing with the challenge of the stem effect in PSDs: twin fibres, spectral discrimination and air core light guide. The authors pointed out that the twin fibres approach enables the subtraction of the stem effect under controlled conditions but is unsuitable for use with modern treatment modalities since the twin fibres cannot generate an equal magnitude of Cerenkov signal in situations where the central beam axis angle changes or where high dose gradients are present. The spectral discrimination method and the air core light guide are both capable of correctly dealing with the stem effect and the selection of the method can therefore be based on the specific requirement of the clinical task, like dosimetric accuracy, acquisition time, the warm-up period, the complexity of calibration and the mechanical flexibility of the dosimeter.

Archambault et al. (2006) compared the twin fibres method with the optical filtering and spectral discrimination approaches using PSDs. They also highlighted that the presence of a second optical fibre required in the twin fibre approach has an impact on the spatial resolution in the case of strong dose gradients. The optical filtering method gave, as expected, the poorest results considering the blue and green emissions of the scintillators used (BCF-12 and BCF-60), overlapped with the stem effect spectrum. The spectral discrimination approach was found to be suitable for precise dose evaluation in the irradiation set-up employed.

In (Beierholm et al., 2008) a direct comparison between two different types of scintillators (Al_2O_3:C and BCF-12), together with two different methods of stem removal is proposed. Time gating and spectral discrimination were considered. Concerning these methods, the authors concluded that the time gating approach was able to remove the stem effect completely from Al_2O_3:C measurements, but can only be used for pulsed irradiation beams. The spectral discrimination method was more complex but can be used for both Al_2O_3:C and BCF-12 probes, also for non-pulsed irradiations.

In the frame to investigate whether or not a stem effect removal technique was necessary when performing ^{192}Ir HDR brachytherapy *in vivo* dosimetry using a BCF-60 PSD, Therriault-Proulx et al. (2011) applied both the optical filtration approach and the spectral discrimination method. The results proved that it was necessary to implement a stem effect removal technique in order to perform accurate in-vivo dosimetry during ^{192}Ir HDR brachytherapy treatments and that the spectral discrimination method provided more accurate results than the optical filtration one.

Taking into account the experimental evidences reported in the literature, the main features of the various stem effect removal methods are outlined in Table 2.

3. Application of RL-based FODs in radiotherapy

3.1. Small-field dosimetry

Clinical radiation fields are classified as small-fields when any of the following conditions occur: 1) lateral-charged-particle-equilibrium (LCPE) does not exist along the central axis, 2) the radiation source is partially occluded by collimation, or 3) the dosimeter's size is similar or larger than the field's cross-section (IAEA, 2017). With small-field conditions come several challenges that complicate dosimetry. Source occlusion and the breakdown of LCPE produces non-uniform regions of fluence in, changes in the energy spectrum of, and significant lateral dose gradients throughout the delivered radiation field (IAEA, 2017). When a dosimeter's sensitive volume occupies non-uniform fluence regions in the radiation field, volume-averaging can perturb the proportionality between dose absorbed by the sensitive volume and point-dose at the effective point of measurement (EPOM) (IAEA, 2017). For dosimeters comprised of materials with non-water-like densities, their presence in these non-uniform regions causes fluence perturbations that can alter the dose absorbed by the sensitive volume (Scott et al., 2012). The breakdown of LCPE increases the mean photon and electron energy along the field's central axis, with these energies dependent on field size

Table 2
Methods for stem effect correction and their main features.

Method for stem effect correction	Main features
Twin fibre	- Suitable for any type of scintillator - Less accuracy for radiation scenarios typical of modern RT
Optical filtering	- Most suitable for long-wavelength emitting scintillators - Residual stem effect component after the optical filtration generally not negligible, unless scintillators with infrared emission are used
Spectral discrimination	- Provides complete stem effect removal using well-established VIS-emitting plastic scintillators - Requires a preliminary calibration procedure which determines the precision and accuracy of the stem effect correction - Formalism that can be extended to implement *multi-point FODs* - PSDs using this method commercially available
Time discrimination	- Suitable for pulsed radiation beams - Application of the method to PSDs still challenging
Air core light guide	- Prevents the generation of the stem effect in the region of the primary radiation beam - Higher mechanical rigidity due to the presence of the air light guide - Eventual residual stem effect generated by scattered radiation to be removed
Real-time OSL	- Inherently corrects the stem effect - Many inorganic materials require accumulated dose correction

(Sánchez-Doblado et al., 2003). For non-water-equivalent dosimeters, the changes in the radiation field's energy spectrum causes perturbations of dose-response due to the dosimeter's energy dependence.

Corrections are therefore required for combinations of these perturbations to ensure accurate dosimetry. The corresponding correction factors, k_Ω, are characteristic of a given dosimeter, such that $k_\Omega = 1$ indicates that no corrections are required (IAEA, 2017). A dosimeter's correction factors depend on several factors such as the field size (as defined by the Full Width at Half Maximum (FWHM) of off-axis profiles), beam quality, depth of measurement, off-axis position, Source-Surface Distance (SSD)/Source-Axis Distance (SAD) and detector orientation. Given the complex nature of detector-specific correction factors, potential small-field dosimeters should be investigated by means of full Monte Carlo simulation and experimental validation prior to their clinical application (IAEA, 2017).

3.1.1. Small-field dosimetry with PSDs

Although there are many characterisation studies of inorganic scintillators based FODs conducted by irradiating the devices with even small radiation fields (e.g. Mones et al., 2008; Martínez et al., 2017; Veronese et al., 2017; Nascimento et al., 2018), from a clinical point of view, the greatest interest in this field is in PSDs due to their better water-equivalence. In fact, water-equivalent PSDs have gained much interest for clinical small-field dosimetry, being theoretically immune to the density-induced fluence and energy-dependence perturbations. Additionally, their scintillator sensitive volumes can be made small to mitigate volume averaging. The main results on small-fields dosimetry obtained with PSDs will then be reported below, with particular focus on the systems currently on the market.

Through Monte Carlo simulation, Wang and Beddar (2011) studied the proportionality between the mean dose absorbed by PSDs and the point doses absorbed by water at the EPOM (Wang and Beddar, 2011). With length of the sensitive region $\leq$2 mm, variations in proportionality were limited to 1–2 % for square fields between 0.5 cm by 0.5 cm and 10 cm by 10 cm, independent of orientation. Gagnon et al. (2012) and Ralston et al. (2012) applied in-house PSDs for the experimental measurement of small-field output factors, comparing PSD results with EBT2 measured output factors. Across both studies, the in-house PSDs had mean differences with respect to EBT2 film of 1.3 % in the study by Gagnon et al. (2012), and 0.2 % in the study by Ralston et al. (2012).

Morin et al. (2013) compared several commercial stereotactic detectors with two home-made PSDs manufactured using cylindrical scintillating fibres as sensitive volumes (diameters of 0.5 mm and 1 mm, length of 1 mm). Measurements of total scatter factors and dose profiles on a CyberKnife system were performed and the measured total scatter factors were compared with those of Monte Carlo studies. Fig. 3 shows the relative total scatter factors difference normalized to Monte Carlo, related to the smallest fields obtained by using collimators of diameters equal to 5.0 mm, 7.5 mm and 10 mm. The results of this study demonstrated that PSDs measurements provided the best agreement with Monte Carlo simulations among all the detectors investigated. Furthermore, the comparisons of the two PSDs with different diameters perpendicular to the radiation beam suggested that using a 1.0-mm detector results in a negligible volume-averaging effect (≈1%) down to a field size of 5 mm (Morin et al., 2013).

Gingras et al. (2021) applied the commercial Hyperscint RP200 (MedScint, Canada) for the measurement of field output factors for circular collimators with diameters down to 0.5 cm and MLC-defined fields as small as 0.5 cm by 0.5 cm, compared with a microdiamond, stereotactic diode and compact ionization chamber. With all reference dosimeters corrected and no corrections applied to the PSD, PSD field output factors were within 0.7 % of all corrected data (Gingras et al., 2021).

A wealth of literature has investigated the first small-field compatible commercial PSD, Exradin W1 (Standard Imaging, USA) for small-field dosimetry. Kamio and Bouchard (2014) and Papaconstadopoulos et al. (2014, 2017) applied full Monte Carlo simulations to determine central-axis correction factors for several small-field dosimeters including the Exradin W1. In both studies, Exradin W1's correction factors were within 1 % of $k_\Omega = 1$ for field sizes down to 1 cm by 1 cm, independently of dosimeter orientation. Francescon et al. (2014) applied Exradin W1 for the measurement of off-axis profiles, PDDs and Tissue Maximum Ratio (TMR), and derived correction factors through comparison with Monte Carlo simulations. For stereotactic cones with diameters as small as 5 mm, correction factors were within 1 % of $k_\Omega = 1$ for off-axis profiles, and were within 1.5% of $k_\Omega = 1$ for PDDs and TMRs. Experimental studies using the Exradin W1 for scanning measurements reported that the stem correction method is energy dependent (Beierholm et al., 2014; Carrasco et al., 2015; Dimitriadis et al., 2017), and as a result should not be applied for scanning measurements (Underwood et al., 2015). For this reason, it is recommended that the Exradin W1 should be applied only for point-based measurements, and that its calibration factor be recalculated for each beam quality.

To address the scanning measurement limitations of the Exradin W1, Standard Imaging developed and released the Exradin W2, a scanning measurement compatible iteration on the Exradin W1. Experimental studies by Galavis et al. (2019) and Jacqmin et al. (2022) verified that the W2 retained the dosimetric properties of the Exradin W1 in broad beams and small-fields. Jacqmin et al. (2022) reported that the Exradin W2's calibration factor for its stem-correction method was energy dependent, as reported for the Exradin W1. A dependence on polar angle was also observed (Jacqmin et al., 2022). Studies by Galavis et al. (2019), Jacqmin et al. (2022) and Okamura et al. (2022) verified that the Exradin W2 remains accurate during scanning measurements. From these studies, the authors recommended the use of Exradin W2 as a relative dosimeter through point-based and scanning-measurements. As an example, Fig. 4 shows the PDD and relative dose profile of a CyberKnife circular beam (diameter equal to 1 cm), measured by Okamura et al. (2022) using the Exradin W2 FOD (Standard Imaging, USA), and compared with the results obtained with a diode (60018 PTW, Germany) and with a microdiamond (60019 PTW, Germany). Very similar curves were obtained.

In conclusion, the literature achieves consensus on the application of

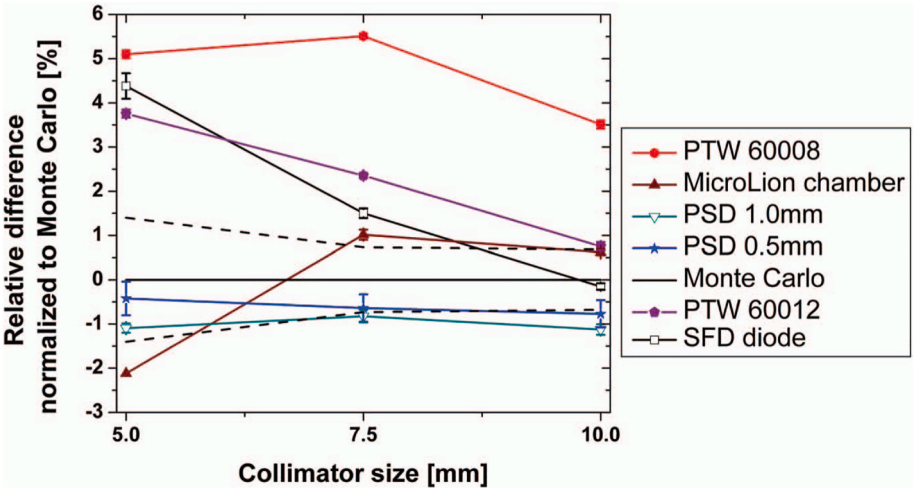

Fig. 3. Relative total scatter factors difference normalized to Monte Carlo, for circular fields provided by a CyberKnife system. Results obtained with various commercial stereotactic detectors and with two PSD prototypes are shown (Reproduced from Morin et al., 2013).

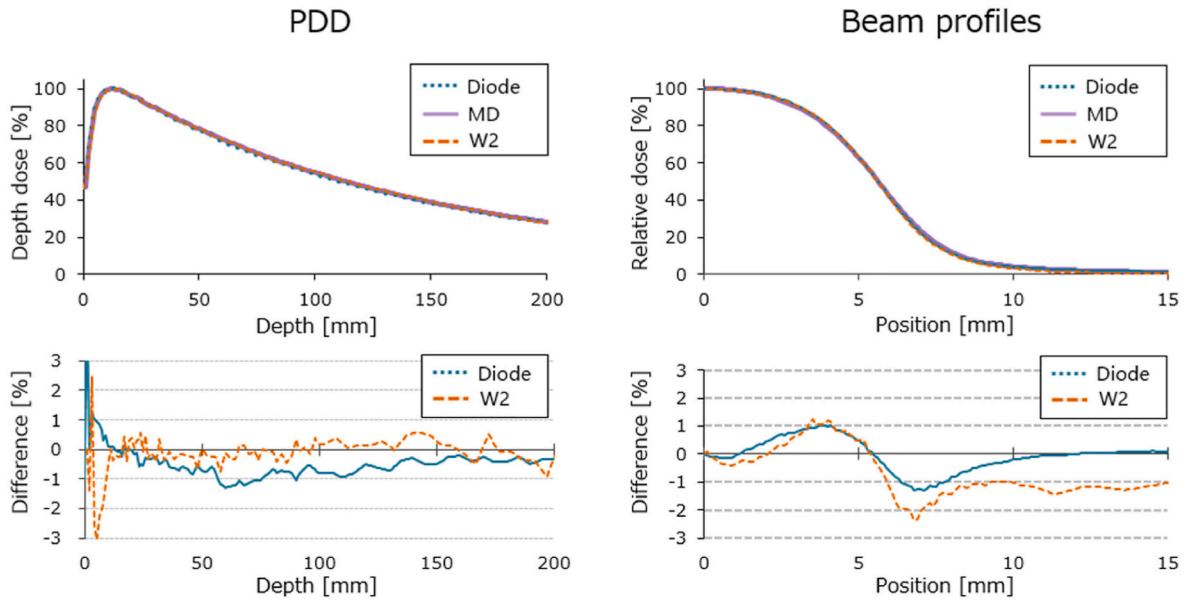

Fig. 4. PDD curves and profiles of a 1 cm circular beam delivered by a CyberKnife unit, measured with various detectors. The lower panels show the difference from the values measured with the microdiamond (Reproduced from Okamura et al., 2022).

PSDs for small-field dosimetry. Provided PSDs have sensitive volumes small enough to negate the volume averaging effect in each small-field and they can be considered as correctionless for relative dosimetry. Prior to clinical dosimetry, the accuracy of the PSD should be evaluated to verify that it can be applied without correction. Clinical small-field dosimetry should be handled by those experienced with PSDs due to the unique challenges that arise with stem-correction.

3.2. In-vivo dosimetry

In radiotherapy, it is critically important to deliver the required dose to the target while sparing the health tissues. In order to verify if an optimised dose distribution has been achieved, real-time in-vivo dosimeters which can be placed directly at the target would be necessary. With in-vivo dosimetry, the doses delivered during each treatment session of individual patients can be verified and recorded, so any significant errors can be detected and identified and taken into account in subsequent treatment fractions.

In-vivo dosimetry can also be applied for online dose-guided adaptive radiotherapy to further improve clinical outcomes. In-vivo dosimetry is critical for verifying the dose delivery of advanced external beam treatment techniques, such as intensity-modulated radiation therapy (IMRT), stereotactic body radiotherapy (SBRT) and volumetric-modulated arc therapy (VMAT), as well as in brachytherapy. It is also useful for developing new radiotherapy modalities, including proton and heavy-ion radiotherapies as well as FLASH RT where extremely high dose rates are utilised. A number of international organizations (including the IAEA, ICRP, and WHO) and major professional societies in radiation oncology (such as AAPM, ESTRO) recommend in-vivo dosimetry to be systematically implemented.

For any clinical in-vivo dosimeters, the following factors have to be considered: energy dependence, dose rate, temperature, angle dependence, water/tissue-equivalence, fast response, small sensitive volume (high dose gradient, skin dose measurements), field size dependence, response changes with accumulated dose, lifetime, cost, easy to use and handle, calibration and recalibration, interference to other

functionalities (e.g. MRI imaging), cabling and EM interference, correction and conversion factors.

3.2.1. *In-vivo dosimetry with FODs*

The unique features of FODs, including small size, tissue equivalency for PSDs, good sensitivity and wide dynamic range, real-time output, energy and angle independence, and immunity to electromagnetic interferences, make them one of best choices for in-vivo dosimetry.

The potential applications of FODs for in-vivo dosimetry have been realised since the early development stage of FODs and various schemes and systems have been developed and tested in phantom or preclinical settings. The early research and development of FODs for in-vivo dosimetry can be found from a number of review articles (Mijnheer et al., 2013; Beaulieu and Beddar, 2016; Woulfe et al., 2016; Fonseca et al., 2020). Here we present an overview of the most recent developments of FODs and their in-vivo applications in conventional and newly developed external beam radiotherapies as well as in brachytherapy, with a focus on the in-vivo FODs in clinical applications for animals and human patients.

The small sensitive volumes of FODs make them extremely attractive and promising for in-vivo dosimetry in external radiotherapy applications. As the sensitive volumes of FODs are usually in 1 mm by 1 mm by 1 mm ranges, they can be treated as point detectors. Also, if plastic scintillators are employed, nearly tissue equivalent PSDs can be obtained. *In vivo* dosimetry with FODs can be achieved by placing the sensing part on the skin surface of the patient to measure the entrance and exit doses to evaluate the dose delivered to the target. In addition, the measured entrance dose can be utilised to detect possible treatment set-up errors and to identify incorrect use of patient positioning devices, and meanwhile the exit dose will provide valuable information to estimate errors caused by patient anatomical variations and possible errors associated with the treatment planning system algorithm.

For external radiotherapy, truly in-vivo dosimetry means that the dose measurements are performed invasively. In 2014, Wootton et al. (2014) designed and constructed PSDs to monitor dose to the rectal wall in patients undergoing IMRT for prostate cancer. The PSDs were attached to the surface of endorectal balloons used for prostate immobilization to place the PSDs in contact with the rectal wall at or near the targets. With the 142 dose measurements on five patents, it was demonstrated that patients could tolerate the PSDs well and the normal treatment workflow would not be compromised. The authors compared the measured doses with the calculated doses (see Fig. 5) and concluded that the PSD system they developed could provide real-time in-vivo dosimetry with excellent accuracy and reusability.

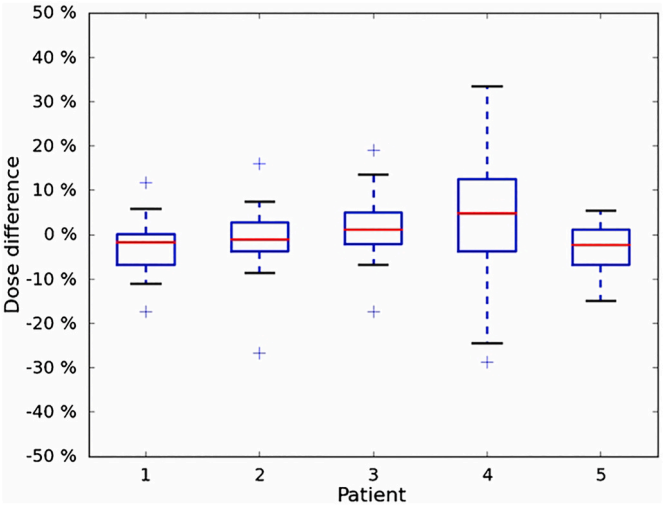

Fig. 5. Boxplot showing the difference between the doses to the rectal wall measured by the PSDs and the calculated doses at the same points in 5 patients undergoing IMRT for prostate cancer (Reproduced from Wootton et al., 2014).

In 2016, clinical tests with an FDA approved in-vivo dosimetry system using plastic scintillating detectors were carried out (Cantley et al., 2016). In this case, the PSDs were also placed in an endorectal balloon to provide real-time in-vivo dosimetry for prostatic rectal interfaces and were tested for use with SBRT. A single patient was treated with a total dose of 36.25 Gy given in 5 fractions. It was found that the measured doses were in an agreement with the computed/planned doses but with an average difference of 6%. The authors attributed the uncertainty to the detector location and the variation in the placement of a new balloon prior to each fraction during the SBRT in which sharp dose falloff near the penumbra along the rectal wall existed. Although only a single patient was involved in the trial, the use of a real-time in-vivo dosimeter provided a level of safety and improved confidence in treatment delivery.

In a review paper by Esposito et al. (2020) the performances of in-vivo point dosimeters available for SBRT and VMAT treatments have been analysed and compared, and it is pointed out that PSDs have the advantages in terms of dose measurement accuracy.

In-vivo surface dosimetry using a PSD system carried out in a preclinical image-guided irradiator was reported by Le Deroff et al. (2020). Dose measurements were performed at the surfaces of PMMA phantom and rats in small radiation fields (5–10 mm). Results show that the discrepancy between the planned and measured doses for the phantom irradiations was 5%. For the animal irradiations, differences from −3.3% to 8.8% were reported, showing that care should be taken when applying PSDs in small-fields and at low energy radiations.

Schoepper et al. (2022) conducted in-vivo dosimetry tests on dogs by using the Hyperscint-RP100 scintillation dosimetry research platform (Hyperscint-RP100, Medscint Inc., Quebec, Canada) and a conventional LINAC. They not only achieved high accuracies in the measurements of field size, depth dose, dose rate as well as angularity, also demonstrated that the PSD device correctly detected the treatment error when the animal heads were intentionally laterally shifted.

It has been demonstrated that FODs are valuable tools as the real-time *in vivo* dosimeters in internal RT and brachytherapy.

In 2011, a PSD system was designed and applied to measure the urethral dose during HDR brachytherapy treatment of the prostate (Suchowerska et al., 2011). With a group of 24 patients, a maximum measured dose departure of 9% from the calculated dose was observed, which demonstrated that the dosimeter always measures the dose in the urethra, despite any movements of the urethra relative to the implant. Therefore, it is recommended that patient response be correlated with the measured rather than the calculated dose.

Kertzscher et al. (2014) designed an Al_2O_3:C based FOD and developed an adaptive error detection algorithm (AEDA) for real-time in-vivo point dosimetry for HDR brachytherapy. The authors demonstrated that the AEDA could correctly identify both true and false error scenarios, relying on positional dosimeter stability rather than accuracy, and they concluded that the AEDA could offer guidance in decision making in the event of potential errors detected with real-time in-vivo point dosimetry.

Kertzscher and Beddar (2019) investigated the capability of different RL-based FODs for in-vivo dosimetry in brachytherapy. The authors considered five different inorganic scintillation materials (ruby Al_2O_3:Cr, a mixture of Y_2O_3:Eu and YVO_4:Eu, ZnSe:O, and CsI:Tl) and compared them with PSDs based on BCF-12 and BCF-60. The results demonstrated that ZnSe:O exhibited the most favourable characteristics over the various investigated inorganic scintillators. Therefore, ZnSe:O based FODs are promising for patient safety monitoring during brachytherapy treatments, provided that energy dependence is accounted for.

Johansen et al. (2019) performed in-vivo dosimetry as part of the clinical workflow in 2D HDR prostate cancer treatments using a FOD with a RL crystal of Al_2O_3:C. With the recorded real-time dose rates over 20 patients and during a period of one year, the dwell times were assessed with high accuracy with the use of time resolved in-vivo

dosimetry over more than 3000 dwell times.

Another study on dwell time measurements with a PSD system (PRODOSE, NU-RISE, Ilhavo, Portugal) was reported by Herreros et al. (2022). The patient measurements were carried out in 20 sessions of 17 patients undergoing postoperative endometrial carcinoma brachytherapy. A relative standard deviation below 1% for the measured dwell times and a relative standard deviation lower than 1.2% for the PSD sensitivity with accumulated absorbed dose were achieved.

As in-vivo dosimeters, FODs were also employed for 3D source tracking and error detection in HDR brachytherapy (Jørgensen et al., 2021; Linares Rosales et al., 2021). Using an Al_2O_3:C based FOD as the in-vivo RL dosimetry system, Jørgensen et al. (2021) performed both source tracking and 3D dose reconstruction functionalities for HDR prostate brachytherapy. With a cohort of 18 patients and a total number of 352 treatment catheters, they evaluated the robustness of the treatments against observed geometric variations and concluded that the 3D dose reconstruction for HDR prostate brachytherapy is feasible.

Time-resolved dosimetry was performed by Linares Rosales et al. (2021) in a water phantom during HDR brachytherapy irradiation with ^{192}Ir source using two different FODs. The first was based on three PSDs (BCF-10, BCF-12, and BCF-60) and the second on a single inorganic crystal of CsI:Tl. The combination of these two independent scintillator dosimetry systems demonstrated to be a promising approach for real-time 3D source tracking in HDR brachytherapy.

More recently, Birajdar et al. (2023) developed a ruby-based FOD for in-vivo real-time dose rate measurement during internal beta radiation therapy (SIRT) and characterised it using a 6 MeV electron beam and a positron-emitting radionuclide fluorine-18.

The feasibility of using FOD consisting of a terbium-doped gadolinium oxysulfide (Gd_2O_2S:Tb) as a real-time in-vivo dosimetry solution for applications in low-dose-rate (LDR) prostate brachytherapy has also been explored (Martyn et al., 2023).

All above mentioned studies demonstrate that FOD systems are useful tools for quality assurance and in-vivo in brachytherapy treatments.

In summary, the rapid progress in research and development of FODs has provided opportunities for achieving in-vivo dosimetry in both existing radiotherapy modalities and new emerging RT technologies. With the unique features of FODs, we expect to see more clinical applications of these detectors as in-vivo dosimeters in the near future.

3.3. Hadrontherapy

Hadrontherapy, also known as particle therapy, is an advanced form of cancer treatment that utilises hadrons for the treatments of patients affected by oncological pathologies. The primary advantage of hadrontherapy over conventional radiotherapy lies in its ability to deliver highly focused radiation to the tumour while sparing surrounding healthy tissues. In fact, unlike traditional X-ray radiation used in conventional radiotherapy, charged particles like protons, carbon ions or other heavy ions deposit most of their energy precisely at the tumour site, minimizing damage to adjacent normal tissues. This characteristic reduces the risk of side effects and allows for increased treatment doses, potentially enhancing therapeutic outcomes. Furthermore, thanks to the radiobiological characteristics of heavy ions, hadrontherapy is particularly suited for treating radio-resistant or inoperable tumours (Rossi, 2022).

In recent years, there has been a noticeable increase in the number of hadrontherapy facilities worldwide. Today, more than 100 proton centres are widely spread in the world while the number of centres able to deliver clinical beams of carbon ions is still limited to one dozen, as reported by the (Particle Therapy Co-Operative Group Website,).

A special type of hadrontherapy is Boron Neutron Capture Therapy (BCNT), a technique that involves introducing boron compounds into cancer cells and then irradiating the tumour with neutrons, causing the boron to release alpha particles that specifically damage the cancer cells (Jin et al., 2022). Recently, the interest in BNCT re-emerged owing to the development and diffusion of accelerator-based neutron sources with characteristics suited for this particular treatment modality (Rossi, 2022).

Due to the peculiarities of these types of radiation therapies, dosimetry, monitoring and quality assurance of radiotherapy beams are of paramount importance for patient safety and treatment outcome. Numerous dosimetry and detection systems have been implemented for these purposes, and scintillators in their various forms also play a key role.

3.3.1. FODs in hadrontherapy

FODs have been applied extensively to the area of hadrontherapy dosimetry. However, one major issue is the dependence to linear energy transfer (LET), referred to as ionization quenching. Ionization quenching is where signal degradation is observed in areas of high LET. This is a particular issue when measuring a PDD curve. Uncorrected, ionization quenching can lead to a reduced estimate of the dose in the Bragg peak.

3.3.1.1. Bare optical fibres in hadrontherapy. Several studies available in the literature are related to the use of bare optical fibres (i.e. lacking a scintillating element), either plastic or silica, utilised for proton beam monitoring and characterisation. Plastic optical fibres have been reported to have a linear dose response, high spatial resolution and exhibit minimal quenching for proton dosimetry (Son et al., 2017; Won Jang et al., 2012). The origin of the light emitted by plastic optical fibre dosimeters has had some discussion, with the most recent reports showing that the light generated is both fluorescence and Cerenkov (Helo et al., 2014; Christensen et al., 2019; Darafsheh et al., 2016, 2017a; Won Jang et al., 2012).

Silica optical fibres have also been shown to have similar properties as the plastic optical fibres. In the case of silica optical fibres, two main emission peaks have been observed at 460 nm and 650 nm (Darafsheh et al., 2017b, 2018). It was found that while the 650 nm peak had a linear dose dependence and quenching free response, the 460 nm peak did not and that the ratio of the peaks varied with proton penetration depth in a material at the Bragg peak for 100 MeV proton (Darafsheh et al., 2017b, 2017c, 2018). This was concluded to possibly be a linear energy transfer dependence. However other studies have shown a silica optical fibre response with a sensitivity to accumulated dose (Santos and Depauw, 2020).

Recently, significant changes to the emission spectrum and continuous increase in response for PMMA and silica optical fibres under constant dose rate exposures, have been reported in proton beams of 16.5 MeV (Asp et al., 2019). Similar spectral changes and an increasing response have been previously reported for silica optical fibres but were considered to be a linear energy transfer (LET) dependence (Darafsheh et al., 2017c, 2018).

3.3.1.2. PSDs in hadrontherapy. The use of PSDs to characterise proton beams has been reported since the early 2000's (Torrisi, 2000), where the quenching effect was clearly observed with a conclusion that BC-400 scintillator could not be used to measure modulated proton beams without correction factors. The quenching effect is an under response to high LET radiation, which is most evident when measuring the Bragg peak. This non-linear light output response to linear energy transfer was first reported by Birks (1951) as:

$$\frac{dL}{dz} = \frac{S}{\left|\frac{dE}{dz}\right|^{-1} + kB}$$

where dL is the light yield per unit length dz, $\frac{dE}{dz}$ is the LET, S is the scintillation constant for the material and kB is Birks' constant.

A majority of studies investigate the impact of the quenching effect and using Birks and other models to correct it in the measurement of the

Bragg peak (Archambault et al., 2008; Christensen et al., 2019, 2020; Kelleter and Jolly, 2020; Penner et al., 2023; Wang et al., 2012). Some investigators have looked to utilise the quenching effect to also measure LET in real-time (Alsanea et al., 2018).

BCF-12 based PSDs were utilised by Wootton et al. (2015) to measure the absolute entrance dose of a passively scattered proton beams with an energy range between 140 and 250 MeV. The performance of the commercially available Exradin W1 PSD (Standard Imaging, USA) was also reported for small proton fields commonly used in ocular treatments (Hoehr et al., 2018).

Matrices and arrays of plastic scintillating fibres were used for the construction of various detectors useful for QA and dosimetry in hadrontherapy, such as a real-time proton and carbon ion radiography system (Lo Presti et al., 2016), a prototype detector for dose verification measurements in proton therapy (Lee et al., 2013) and a charged fragment tracker for beam range online monitoring in hadrontherapy treatments (Mattei et al., 2018, 2020; Traini et al., 2019).

Finally, FODs produced with polystyrene-based plastic scintillators enriched with boron were used for measuring the depth-dose distribution within a water phantom at the Russian BNCT facility of the Budker Institute of Nuclear Physics (Bykov et al., 2021).

3.3.1.3. Inorganic scintillators based FODs in hadrontherapy. A number of inorganic materials have been investigated for FODs to be used in hadrontherapy. Al_2O_3:C was one of the first inorganic materials tested for proton and carbon ion beams dosimetry (Andersen et al., 2007; de Freitas Nascimento et al., 2022; Nascimento et al., 2015, ; Klein et al., 2011). Since then, Ce-doped, N-doped, B-doped, Gd-doped, Cu-doped, P-doped and Sb-doped silica fibres have been reported for proton beam dosimetry and monitoring (Akchurin et al., 2020; Auger et al., 2016; Braccini et al., 2012; Girard et al., 2019; Hoehr et al., 2018, 2019, 2020; Olusoji et al., 2021; Savard et al., 2018; Veronese et al., 2010).

BeO ceramic, Gd_2O_2S:Tb and (Zn, Cd)S:Ag have also been investigated for proton dosimetry (Metzner et al., 2022; Penner et al., 2018; Safai et al., 2004; Teichmann et al., 2018, 2019). A recent study utilised the spectral changes in the RL at different depths to determine a depth dependent correction factor. This method showed promise in correcting for the quenching observed in BeO ceramics (Metzner et al., 2022).

Similar to plastic scintillators, ionization quenching also impacts all inorganic scintillators to varying degrees. Proper methods of corrections of the RL response are consequently required. Examples of quenching phenomena observed by de Freitas Nascimento et al. (2022) in different types of Al_2O_3:C based FODs irradiated with various particle beams are shown in Fig. 6.

3.4. MRI-LINAC dosimetry

MRI-LINAC treatment units are comprised of an MRI-scanner and a LINAC. There are currently two established setups for MRI-LINACs: the perpendicular MRI-LINAC setup (with photon beam aligned perpendicular to the magnetic field), and the in-line MRI-LINAC setup (with photon beam aligned parallel to the magnetic field). There currently exist four MRI-LINAC systems, each with different combinations of MRI-LINAC setup, magnetic field strength, and photon beam energy. These characteristics of these systems are detailed in Table 3.

With the envelopment of the radiation field by magnetic field,

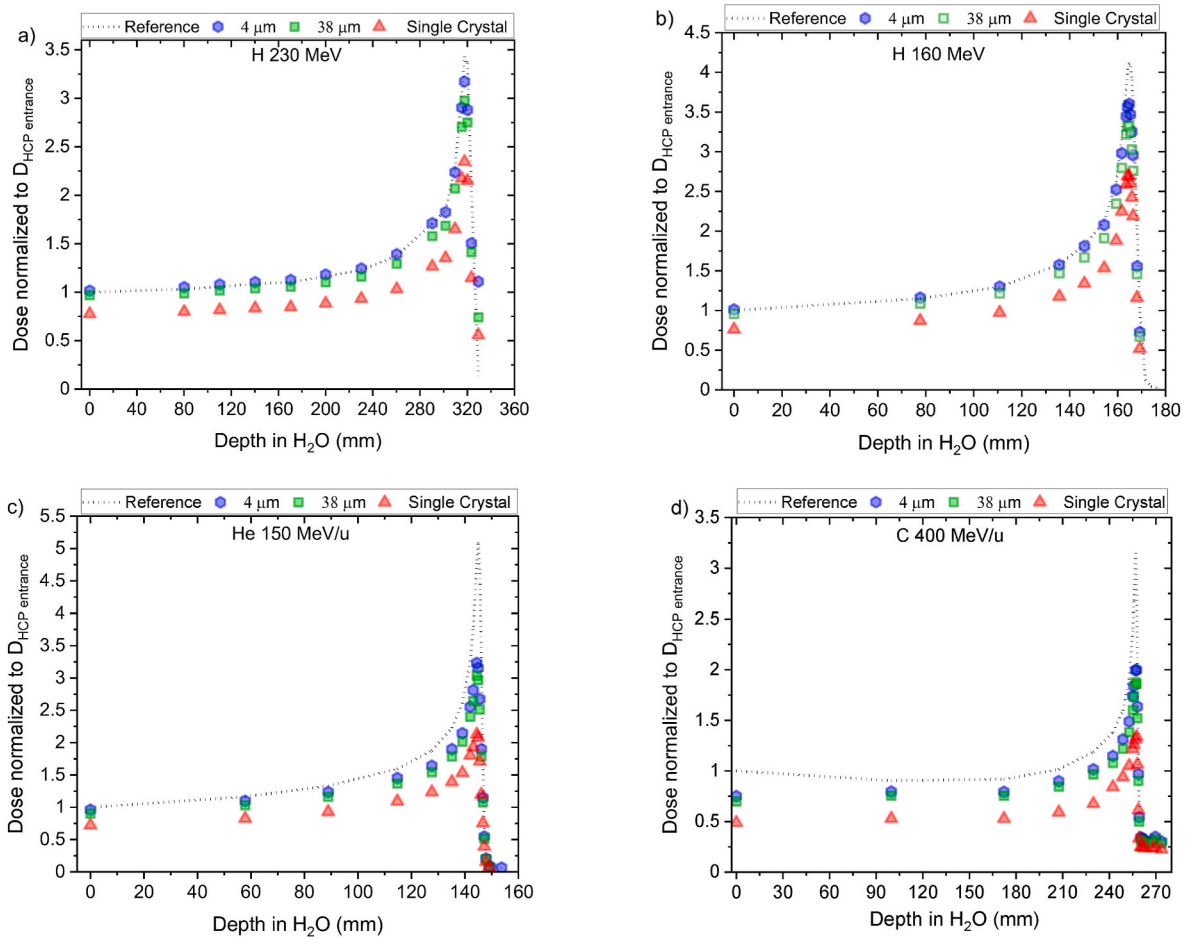

Fig. 6. Bragg curves of particle beams measured with Al_2O_3:C based FODs characterised by various geometries of the scintillating element (single crystal and droplets containing powder of different grain size). Reference curves were obtained with a Markus ionization chamber. (Reproduced from de Freitas Nascimento et al., 2022).

Table 3
Characteristics of the current MRI-LINAC systems. With regards to photon beam energies, FFF corresponds to flattening filter free beams, and FF corresponds to beam with flattening filter.

MRI-LINAC system	Setup	Magnetic field strength (T)	Photon beam energy (MV)
Elekta Unity (Lagendijk et al., 2014)	Perpendicular	1.5	7 MV FFF
ViewRay MRIdian (Mutic and Dempsey, 2014)	Perpendicular	0.35	6 MV FFF
Aurora RT (Fallone, 2014)	In-line	0.6	6 MV FF
Australian MRI-LINAC (Keall et al., 2014)	In-line	1.0	6 MV FF

charged particles are acted upon by a Lorentz force, causing them to follow helicoidal trajectories with directionality dependent on the MRI-LINAC setup. Macroscopically, the magnetic focusing of charged particles can manifest changes in the dose distributions delivered, specific to the MRI-LINAC setup. The characteristics of these effects have complex dependences on magnetic field strength, photon beam energy, medium density, phantom geometry and field size (Huang et al., 2023).

For perpendicular MRI-LINACs, charged particles follow helicoidal trajectories focused orthogonal to the photon beam and magnetic field. This reduces electron penetration depth (Raaymakers et al., 2004) and laterally skews and shortens dose-kernels (Gargett et al., 2015), causing off-axis profiles to become laterally skewed (Raaymakers et al., 2004). The magnetic focusing of contaminant electrons and head scatter reduces surface doses along the central axis (Keyvanloo et al., 2012). With regards to charged particle trajectories, the radius of gyration is dependent on density. This gives rise to the electron return effect (Raaijmakers et al., 2005), in which charged particles exiting from high-density materials into low-density materials experience drastically reduced gyration radii, re-penetrating the high-density materials near their point of exit and causing changes to the dose distributions (Raaijmakers et al., 2005).

For in-line MRI-LINACs, charged particles are directed along helicoidal trajectories focused parallel to the photon beam and magnetic field. This reduces electron penetration depth and reduces the lateral range of secondary charged particles (Oborn et al., 2016), causing dose-kernels to shorten and narrow (Gargett et al., 2015), and penumbrae to narrow (Alnaghy et al., 2018). The magnetic focusing of charged particles from head scatter and contamination is responsible for increased surface doses near the central axis (Oborn et al., 2012).

Dosimeter perturbations also arise with the magnetic focusing of charged particles. For perpendicular MRI-LINACs, charged particle fluences become laterally anisotropic (Bouchard and Bielajew, 2015), causing materials with non-water like densities to perturb charged particle fluences (De Pooter et al., 2015). During dosimetry, fluence perturbations can be induced by any materials in or around the sensitive volume that have dissimilar densities to water (Bielaiew, 1993; De Pooter et al., 2015). For in-line MRI-LINACs, charged particle fluences remain laterally isotropic; consequently, charged-particle fluence perturbations are reduced for in-line MRI-LINACs (Bielaiew, 1993). Many dosimeters experience orientation dependent responses with MRI-LINACs, arising from asymmetrical sensitive volume geometries (Cervantes et al., 2021, 2022). With both MRI-LINAC setups, dosimeters experience a shift in their effective point of measurement (EPOM) (Looe et al., 2017). The severity, prevalence and characteristics of these effects are characteristic of the dosimeter, and dependent on several external factors.

3.4.1. MRI-LINAC dosimetry with PSDs

Water-equivalent PSDs were theorised promising prospects for MRI-LINAC dosimetry, being composed entirely of water-equivalent materials with water-like-densities. Consequently, PSDs are theoretically immune to density induced fluence perturbations for perpendicular MRI-LINACs (De Pooter et al., 2015) and experience EPOM shifts matching those of equivalent volumes of water (Looe et al., 2017). Their non-ferromagnetic compositions prevent perturbations of the MRI scanner's magnetic field, beneficial for patient specific quality assurance dosimetry. Current literature does not achieve consensus on whether the scintillation response is influenced by magnetic fields. Initial studies reported varying magnitudes of increase in response (Bertoldi et al., 1997; Blömker et al., 1992; Cumalat et al., 1990; Stefanowicz et al., 2013), though adequate stem correction methods were not applied in many of these studies. Later studies demonstrated that inadequate stem corrections cause increases in PSD response in the presence of magnetic fields (Simiele et al., 2018; Therriault-Proulx et al., 2018). Therriault-Proulx et al. (2018) studied the effect of the magnetic field on the response of the Exradin W1 PSD (Standard Imaging, USA) and of an in-house PSD system composed of a 3-mm-long BCF-60 scintillating fibre. In all cases, the authors observed an increase of the light intensity as the magnetic field strength increased. This effect was particularly noticeable for a bare fibre (see Fig. 7). With adequate stem corrections, Therriault-Proulx et al. (2018) reported a maximal increase in response of 2.4 % for magnetic field strengths up to 1.5 T, positing that this increase in response arose with an increase in the dose absorbed by the PSD. Further research is required to determine whether scintillation response has a weak magnetic field dependence.

Many studies have reported that the accuracy of stem correction methods can be reduced for MRI-LINACs. The twin-fibres approach can remain accurate with MRI-LINACs (Madden et al. 2019; 2020; 2021b), however, its accuracy can be reduced when applied in fields with significant dose gradients (Simiele et al., 2018). With regards to spectral discrimination methods, the spectral responses of Cerenkov radiation and opticalfibre fluorescence are influenced by magnetic fields. Simiele et al. (2021) reported that optical fibres can produce varying ratios of opticalfibre fluorescence and Cerenkov radiation in the presence of magnetic fields, inducing variations in CLR calibration factors. It was concluded that optical fibres with low fluorescence yields should be used to minimise the variation of CLR calibration factors (Simiele et al., 2021). Time discrimination methods and air-core PSDs have not been investigated with MRI-LINACs; further research is required prior to their clinical application.

Studies performing relative dosimetry for MRI-LINACs with PSDs have demonstrated the promise of PSDs with MRI-LINACs. Madden et al.

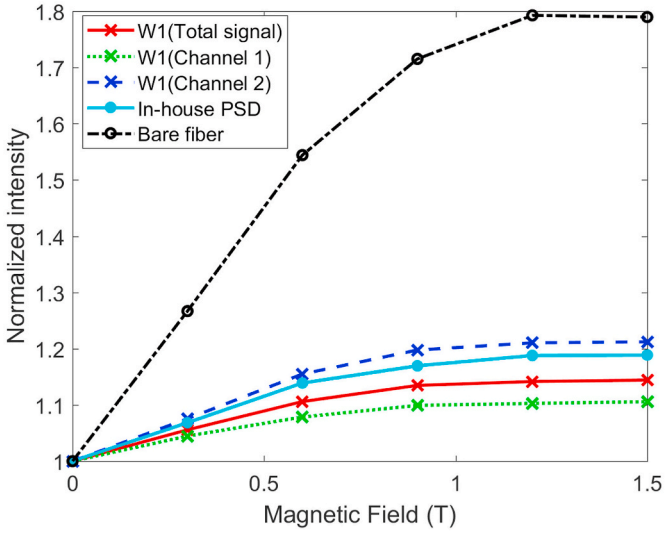

Fig. 7. Normalized light intensity as a function of the magnetic field strength, produced by an irradiated bare fibre, by the Exradin W1 PSD (Standard Imaging, USA) and of an in-house PSD system. For the Exradin W1 PSD, the output of the two channels used to analyse the luminescent signals were considered (see section 2.2.3). (Reproduced from Therriault-Proulx et al., 2018).

(2019, 2020, 2021b) measured output factors, beam profiles and percent depth dose distributions for the Australian MRI-LINAC with an in-house PSD, with PSD measurements generally in good agreement with reference data. Yoon et al. (2019) measured output factors for the ViewRay MRIdian with the Exradin W1, reporting that PSD response was accurate for field sizes $\leq$10.5 cm by 10.5 cm. The authors reported unexplainable deviations in output factor for field sizes >10.5 cm by 10.5 cm and recommended against its use for these field sizes. Klavsen et al. (2022) applied an in-house PSD for real-time dose-verification of a ViewRay MRIdian's gated treatment using a dynamic phantom, demonstrating accurate measurement of dose-per-pulse in real-time. Uijtewaal et al. (2023) applied the commercial Hyperscint RP200 (Medscint, Canada) for scanning water tank measurements with an Elekta Unity. Ferrer et al. (2023) dosimetrically characterised the commercial Blue Physics Model 10 PSD (BluePhysics, USA) with the Elekta Unity and applied it for anthropomorphic head phantom measurements.

To conclude, there is mounting evidence to support that PSDs remain accurate for dosimetry with MRI-LINACs given their water-equivalent densities. Stem correction methods must account for changes in the characteristics of optical fibre fluorescence and Cerenkov radiation that arise in strong magnetic fields. In line with recommendations from other codes of practice, we recommend that PSDs be clinically applied by those familiar with PSDs due to the complexities of stem corrections.

3.5. FLASH and microbeam RT

FLASH RT is a promising, potentially cutting-edge therapy for oncological diseases which relies on delivery of therapeutic doses in less than 1 s using ultra-high dose rates (UHDR), i.e. typically >40 Gy/s (Favaudon et al., 2014.). Several preclinical studies have shown that FLASH RT may strongly decrease normal tissue toxicity while maintaining high tumour control probability compared to conventional (CONV) RT (Gao et al., 2022). However, a comprehensive understanding of the radiobiology mechanisms underlying the FLASH effect are required for the clinical transition of FLASH RT. Radiobiology studies have been conducted with various UHDR radiation beams delivered by different systems, including (i) electron beams obtained by experimental and modified clinical machines, as well as by precommercial and commercial systems, (ii) proton beams and (iii) X-rays generated by synchrotrons and modified X-ray tubes (Ashraf et al., 2020; Bazalova-Carter and Esplen, 2019).

Microbeam Radiation Therapy (MRT) uses synchrotron generated X-ray beams of kilovoltage-energy, which are segmented into an array of narrow, quasi-parallel, micro-planar beams, delivered in a single treatment session, in a scanning mode. The very high in-beam 'peak' dose zones are separated by very low-dose 'valley' regions. These in-beam doses are orders of magnitude greater than those normally delivered in CONV RT (Grotzer et al., 2015).

These novel promising high dose rate RT modalities require novel solutions for dosimetry and beam monitoring. Indeed, the well-established dosimeters currently used in CONV RT have been reported to suffer from saturation effects under UHDR regimes (Esplen et al., 2020; Romano et al., 2022). Recently, important progresses have been achieved in the challenge to extend the working range of various types of real-time dosimeters, like ionization chambers (Di Martino et al., 2022; Gómez et al., 2022) and diamond detectors (Marinelli et al., 2022) towards UHDR beams. Real-time luminescence sensors like Cerenkov and scintillation-based detectors may also have a key role to play in the development of FLASH RT (Ashraf et al., 2020).

3.5.1. FODs in FLASH and microbeam RT

With regards to investigations of FODs in UHDR regimes, various studies were performed aimed to characterise UHDR beams of different qualities using plastic or inorganic scintillators based FODs. Similarly, several studies have investigated the performance of FODs prepared with different scintillating materials under UHDR irradiation regimes, through a direct comparison with other dosimetric systems, and/or Monte Carlo simulations. A non-exhaustive overview of the studies available in the literature, categorised on the basis of the type of radiation used for UHDR irradiation, is given below.

3.5.1.1. Protons. Kanouta et al. (2022) used FODs prepared with sub-millimetric ZnSe:O crystals to measure the time structure and dose rates during in-phantom and in preclinical mouse FLASH experiments performed with pencil scanning proton beams. The study included measurements of individual spot durations and spot transitions times. The comparison between the measured time values and the log-files timing allowed an independent validation of the log-files information, demonstrating the potential of the FODs for quality assurance of proton FLASH treatments. A further characterisation of this system in terms of precision and stem signal was reported in (Kanouta et al., 2023) where the calibrated system was also used for in-vivo measurements in mouse experiments, where mouse legs were irradiated with a constant dose and instantaneous dose rates spanning in the interval 0.08–953 Gy/s. The results showed a high precision and stability of the FOD system and an under-response of the signal for high instantaneous dose rates. The stem effect contribution exceeded 10% when the beam was less than 5 mm from the fibre and more than 18 mm from the scintillator. Despite this large relative contribution of the stem effect at large distances from the scintillator, its contribution to the overall dose at the point of the detector was considered negligible for the used scanning pattern (Kanouta et al., 2023).

3.5.1.2. Photons. Cecchi et al. (2021) used a PSD (0.5 mm in diameter and 0.47 mm in length) connected to a Hyperscint RP 100 optical reader (Medscint, Canada) to characterise an X-ray tube-based UHDR system. The radiation unit, designed by coupling a conventional X-ray tube with a custom beam shutter, enabled the delivery of short (i.e. <1 s) UHDR irradiations to samples placed close to the tube window. Monte Carlo (MC) simulations were performed to estimate the absorbed doses and dose rates delivered to the PSD using a previously validated model of the irradiator. MC simulations showed good agreement with PSD measurements in terms of beam temporal profile and absorbed dose. A linearity of the PSD response with increasing instantaneous dose rate from 3.1 Gy/s to 118.0 Gy/s was also observed. The overall results proved the efficacy of the characterisation of UHDR X-ray beams by means of PSD measurements coupled with MC modelling.

UHDR X-ray-based radiation unit similar to the one characterised by Cecchi et al. (2021) was used by Shaharuddin et al. (2021) and by Hart et al. (2022) to test the performances of FODs prepared using different scintillating materials. The inorganic scintillators Gd_2O_2S:Tb, La_2O_2S:Tb and La_2O_2S:Eu in form of powder inserted into bore cavities of 0.5 mm diameter at 1- and 2-mm depth obtained in PMMA optical fibres were studied by Shaharuddin et al. (2021). A BCF-10 scintillator and three hybrid lead-doped scintillators (0.97 mm in diameter and 3.6 mm in length) with different concentrations of Pb, C and H were tested by Hart et al. (2022). To account for the stem effect, the HYPERSCINT RP-100 and RP-200 dosimetry research platforms (Medscint, Canada) were employed by Hart et al. (2022) and by Shaharuddin et al. (2021), respectively. In both studies, dose rate response of the PSDs systems was investigated by varying the tube current, and MC simulations were carried out to calculate the dose rate absorbed by the various scintillators. Linear dose rate responses up to dose rate values of approximately 40 Gy/s were measured.

High brilliance X-rays produced in a synchrotron (dose rate of 4435 Gy/s) were used by Archer et al. (2017b, 2017c, 2018c, 2019b) to test the dosimetric performance of PSDs consisting of a thin sheet of BC-400 plastic scintillator optically coupled to the end of a 1 mm core PMMA optical fibre, and covered in Bicron BC-620 reflector paint. The spatial resolution of the PSD was progressively improved by reducing the

thickness of the scintillator from 50 μm to 10 μm. With this geometry, the detector was able to resolve individual 50 μm wide microbeams. Authors pointed out that a significant part of the total light signal collected (equal of approximately 52% in the used irradiation conditions) derived from radioluminescence phenomena originating in the PMMA optical fibre, highlighting the importance of dealing with the stem effect also during PSD-based QA measurements in MRT.

3.5.1.3. Electrons. Poirier et al. (2022) characterised the Hyperscint RP-100 dosimetry system (Medscint, Canada) using 16 MeV UHDR electron beams generated by a converted medical LINAC. The PSD was irradiated in different configurations up to a dose rate of approximately 100 Gy/s, achieved with a dose per pulse of about 0.55 Gy/pulse. The dose-response of the PSD was shown to be linear within ±1% up to 20 Gy at a dose rate of ~ 34.5 Gy/s (dose-per-pulse of about 0.2 Gy/pulse) and to agree with the dose-response curve of measured with radiochromic films at doses per pulse in the range 0.2–0.55 Gy/pulse.

Di Martino et al. (2020) used 10 MeV electron beams generated by a dedicated Intra Operative Radio Therapy (IORT) mobile LINAC converted into a FLASH research machine to investigate dosimeter saturation problems occurring in UHDR irradiation regimes. Different types of detectors were irradiated at increasing dose-per-pulse up to 40 Gy/pulse, using radiochromic films as reference dosimeters. Among the various investigated devices, the Dose Wire Series 100 detector (DoseVue N.V., Belgium) was considered. It was an inorganic based FOD consisting of a hemispherical 0.1 cc active volume of europium-doped yttrium oxide. A progressive loss of linearity of the FOD response with increasing the dose-per-pulse was observed, with a cutoff value between 11 and 36 Gy/pulse, where saturation was no longer correctable.

The loss of linearity as the dose-per-pulse increases is a feature observed in various other studies performed whilst irradiating different FODs with pulsed UHDR electron beams. In fact, such a feature remains one of the main challenges for the possible future use of FODs in electron FLASH beam dosimetry. Morrocchi et al. (2022) tested two different FODs using 9 MeV electron beams produced by an electron FLASH accelerator (Sordina, Italy). One FOD was prepared using as scintillating material a EJ212 plastic scintillator (dimensions 20 by 10 by 2 mm^3) placed at the edge of a PMMA slab of cross section 10 by 10 mm^2, that acted as a light guide. The other FOD consisted of a LYSO crystal (dimensions 2 by 2 by 10 mm^3) coupled with a PMMA optical fibre. The results of the measurements performed by changing the dose-per-pulse suggested that the plastic scintillator has a linear response up to 6 Gy/pulse and the LYSO dosimeter up to 3.5 Gy/pulse. Afterwards, saturation effects were observed for both the FODs.

Using the same electron flash accelerator model employed in (Morrocchi et al., 2022), Vanreusel et al. (2022) performed a preliminary characterization of different FODs based on five different inorganic scintillators: Al_2O_3:C; Al_2O_3:C,Mg; Y_2O_3:Eu; $(C_{38}H_{34}P_2)MnCl_4$ and $(C_{38}H_{34}P_2)MnBr_4$. Millimetric or sub-millimetric probe sizes were considered, according to the scintillator type and form. All the FODs were designed and developed for research purposes in CONV and/or FLASH RT, apart from the two Y_2O_3:Eu based FODs that consisted of a point scintillator of the commercial DoseWire 200 series (DoseVue N.V., Belgium) and in an experimental variant hereof with decreased crystal concentration. For all scintillators, the loss of linearity of the response with increasing the dose-per-pulse was evident below 4 Gy/pulse, except for the $(C_{38}H_{34}P_2)MnCl_4$ and $(C_{38}H_{34}P_2)MnBr_4$ scintillators for which saturation seems to appear at higher dose-per-pulse values.

The study by Vanreusel et al. (2022) also showed how the response of a scintillator with luminescence decay times exceeding the inter-pulse time decreases with increasing the beam pulse repetition frequency. Among the various scintillating materials tested by Vanreusel et al. (2022), Al_2O_3:C and Al_2O_3:C,Mg were the ones most influenced by the pulse repetition frequency used to deliver the UHDR electron beams because of their longer decay time.

In conclusion, various studies have been carried out, and others are in progress, which have highlighted the potential and limitations of different FODs as systems for QA and dosimetry of FLASH radiation beams and MRT. It is worth noting that some aspects still require improvement or remain partially unaddressed. The aspect related to how much the stem effect contributes in UHDR regimes has been highlighted very rarely in the literature. Indeed, most of the tests were carried out with soft X-rays or protons, where the Cerenkov radiation is absent or negligible. Furthermore, the issue of radiation hardness of both the scintillating elements and the light guides exposed to UHDR beams needs further evaluations in order to assess the potential impact in the medium-long term.

All these open challenges may stimulate new research that is likely to become more and more feasible due to the diffusion of new UHDR beam delivery technologies and to the increasing clinical interest in FLASH RT.

4. Conclusions

Many studies have been conducted on FODs in recent years, both in terms of the development of scintillating materials and in terms of the selection, measurement and analysis of the dosimetric signal alone. The results have enabled the development of reliable FOD systems, some of them on the market, which are nowadays valid dosimetric tools in various RT contexts. By virtue of their characteristics, FODs are also likely to find ample space in dosimetry in future RT scenarios.

Various challenges are still to be faced, such as a full comprehension of the effects of magnetic fields in the dosimetric properties of FODs, the development of new correction methods and/or the validation of existing ones required to take into account ionization quenching effects occurring in hadrontherapy applications, the loss of linearity of the RL signal observed under UHDR irradiation regimes.

Furthermore, it is worth remembering that FODs are unique instruments, and by their nature the response may be influenced by factors such as irradiation geometry and beam quality, especially because of their greater sensitivity to the stem effect. For this reason, a complete dosimetric characterisation of FODs, which also allows the user to gain experience and familiarity with these systems, is always recommended prior to their introduction in a new clinical practice.

CRediT authorship contribution statement

Ivan Veronese: Writing – review & editing, Writing – original draft, Supervision, Methodology, Conceptualization. **Claus E. Andersen:** Methodology, Conceptualization. **Enbang Li:** Writing – review & editing, Writing – original draft, Methodology, Conceptualization. **Levi Madden:** Writing – review & editing, Writing – original draft, Methodology, Conceptualization. **Alexandre M.C. Santos:** Writing – review & editing, Writing – original draft, Methodology, Conceptualization.

Declaration of competing interest

The authors declare that they have no known competing financial interests or personal relationships that could have appeared to influence the work reported in this paper.

Data availability

No data was used for the research described in the article.

References

Akchurin, N., Bartosik, N., Damgov, J., Guio, F. De, Dissertori, G., Kendir, E., Kunori, S., Mengke, T., Nessi-Tedaldi, F., Pastrone, N., Pigazzini, S., Yaltkaya, S., 2020. Cerium-doped fused-silica fibers for particle physics detectors. J. Instrum. 15 (3), C03054 https://doi.org/10.1088/1748-0221/15/03/C03054.

Alnaghy, S.J., Begg, J., Causer, T., Alharthi, T., Glaubes, L., Dong, B., George, A., Holloway, L., Metcalfe, P., 2018. Technical Note: penumbral width trimming in solid lung dose profiles for 0.9 and 1.5 T MRI-Linac prototypes. Med. Phys. 45 (1), 479–487. https://doi.org/10.1002/mp.12680.

Alsanea, F., Therriault-Proulx, F., Sawakuchi, G., Beddar, S., 2018. A real-time method to simultaneously measure linear energy transfer and dose for proton therapy using organic scintillators. Med. Phys. 45 (4), 1782–1789. https://doi.org/10.1002/mp.12815.

Andersen, C.E., Damkjær, S.M.S., Kertzscher, G., Greilich, S., Aznar, M.C., 2011. Fiber-coupled radioluminescence dosimetry with saturated Al 2O3:C crystals: characterization in 6 and 18 MV photon beams. Radiat. Meas. 46 (10), 1090–1098. https://doi.org/10.1016/j.radmeas.2011.06.063.

Andersen, C.E., Edmund, J.M., Medin, J., Grusell, E., Jain, M., Mattsson, S., 2007. Medical proton dosimetry using radioluminescence from aluminium oxide crystals attached to optical-fiber cables. Nucl. Instrum. Methods Phys. Res. Sect. A Accel. Spectrom. Detect. Assoc. Equip. 580 (1), 466–468. https://doi.org/10.1016/j.nima.2007.05.129.

Andersen, C.E., Marckmann, C.J., Aznar, M.C., Bøtter-Jensen, L., Kjær-Kristoffersen, F., Medin, J., 2006. An algorithm for real-time dosimetry in intensity-modulated radiation therapy using the radioluminescence signal from Al2O3:C. Radiat. Protect. Dosim. 120 (1–4), 7–13. https://doi.org/10.1093/rpd/nci600.

Archambault, L., Polf, J.C., Beaulieu, L., Beddar, S., 2008. Characterizing the response of miniature scintillation detectors when irradiated with proton beams. Phys. Med. Biol. 53 (7), 1865. https://doi.org/10.1088/0031-9155/53/7/004.

Archambault, L., Sam Beddar, A., Gingras, L., Roy, R., Beaulieu, L., 2006. Measurement accuracy and Cerenkov removal for high performance, high spatial resolution scintillation dosimetry. Med. Phys. 33 (1), 128–135. https://doi.org/10.1118/1.2138010.

Archambault, L., Therriault-Proulx, F., Beddar, S., Beaulieu, L., 2012. A mathematical formalism for hyperspectral, multipoint plastic scintillation detectors. Phys. Med. Biol. 57 (21), 7133–7145. https://doi.org/10.1088/0031-9155/57/21/7133.

Archer, J., Li, E., 2018. Recent advances in photonic dosimeters for medical radiation therapy. Issue 1. In: Frontiers of Optoelectronics, vol. 11. Higher Education Press, pp. 23–29. https://doi.org/10.1007/s12200-018-0759-3.

Archer, J., Li, E., Davis, J., Cameron, M., Rosenfeld, A., Lerch, M., 2019b. High spatial resolution scintillator dosimetry of synchrotron microbeams. Sci. Rep. 9 (1) https://doi.org/10.1038/s41598-019-43349-6.

Archer, J., Li, E., Petasecca, M., Dipuglia, A., Cameron, M., Stevenson, A., Hall, C., Hausermann, D., Rosenfeld, A., Lerch, M., 2017c. X-ray microbeam measurements with a high resolution scintillator fibre-optic dosimeter. Sci. Rep. 7 (1) https://doi.org/10.1038/s41598-017-12697-6.

Archer, J., Li, E., Petasecca, M., Lerch, M., Rosenfeld, A., 2017b. High-resolution fiber-optic dosimeters for microbeam radiation therapy. Med. Phys. 44 (5), 1965–1968. https://doi.org/10.1002/MP.12209.

Archer, J., Li, E., Petasecca, M., Stevenson, A., Livingstone, J., Dipuglia, A., Davis, J., Rosenfeld, A., Lerch, M., 2018c. Synchrotron X-ray microbeam dosimetry with a 20 micrometre resolution scintillator fibre-optic dosimeter. J. Synchrotron Radiat. 25 (3), 826–832. https://doi.org/10.1107/S1600577518003016.

Archer, J., Madden, L., Li, E., Carolan, M., Rosenfeld, A., 2018b. A comparison of temporal Cherenkov separation techniques in pulsed signal scintillator dosimetry. Biomed. Phys. Eng. Exp. 4 (4) https://doi.org/10.1088/2057-1976/aacf56.

Archer, J., Madden, L., Li, E., Carolan, M., Petasecca, M., Metcalfe, P., Rosenfeld, A., 2017a. Temporally separating Cherenkov radiation in a scintillator probe exposed to a pulsed X-ray beam. Phys. Med. 42, 185–188. https://doi.org/10.1016/j.ejmp.2017.09.134.

Archer, J., Madden, L., Li, E., Wilkinson, D., Rosenfeld, A.B., 2019a. An algorithmic approach to single-probe Cherenkov removal in pulsed x-ray beams. Med. Phys. 46 (4), 1833–1839. https://doi.org/10.1002/mp.13383.

Ashraf, M.R., Rahman, M., Zhang, R., Williams, B.B., Gladstone, D.J., Pogue, B.W., Bruza, P., 2020. Dosimetry for flash radiotherapy: a review of tools and the role of radioluminescence and cherenkov emission. In: Frontiers in Physics, vol. 8. Frontiers Media SA. https://doi.org/10.3389/fphy.2020.00328.

Asp, J., Caraça Santos, A.M., Afshar V, S., Qi Zhang, W., Bezak, E., 2019. Evaluation of silica and PMMA optical fibre response when irradiated with 16.5 MeV protons. Physica Medica. Eur. J. Med. Plants 65, 15–20. https://doi.org/10.1016/j.ejmp.2019.08.001.

Auger, M., Braccini, S., Carzaniga, T.S., Ereditato, A., Nesteruk, K.P., Scampoli, P., 2016. A detector based on silica fibers for ion beam monitoring in a wide current range. J. Instrum. 11 (3), P03027. https://doi.org/10.1088/1748-0221/11/03/p03027.

Bazalova-Carter, M., Esplen, N., 2019. On the capabilities of conventional x-ray tubes to deliver ultra-high (FLASH) dose rates. Med. Phys. 46 (12), 5690–5695. https://doi.org/10.1002/mp.13858.

Beaulieu, L., Beddar, S., 2016. Review of plastic and liquid scintillation dosimetry for photon, electron, and proton therapy. Phys. Med. Biol. 61 (20), R305. https://doi.org/10.1088/0031-9155/61/20/R305.

Beddar, A.S., 2007. Plastic scintillation dosimetry and its application to radiotherapy. Radiat. Meas. 41 (Suppl. 1) https://doi.org/10.1016/j.radmeas.2007.01.002.

Beddar, A.S., Mackie, T.R., Attix, F.H., 1992a. Cerenkov light generated in optical fibres and other light pipes irradiated by electron beams. Phys. Med. Biol. 37 (4), 925. https://doi.org/10.1088/0031-9155/37/4/007.

Beddar, A.S., Mackie, T.R., Attix, F.H., 1992b. Water-equivalent plastic scintillation detectors for high-energy beam dosimetry: I. Physical characteristics and theoretical considerations. Phys. Med. Biol. 37 (10), 1883–1900. https://doi.org/10.1088/0031-9155/37/10/006.

Beddar, A.S., Mackie, T.R., Attix, F.H., 1992c. Water-equivalent plastic scintillation detectors for high-energy beam dosimetry: 11. Properties and measurements. Phys. Med. Biol. 37 (10), 1901–1913. https://doi.org/10.1088/0031-9155/37/10/007.

Beierholm, A.R., Andersen, C.E., Lindvold, L.R., Kjær-Kristoffersen, F., Medin, J., 2008. A comparison of BCF-12 organic scintillators and Al2O3:C crystals for real-time medical dosimetry. Radiat. Meas. 43 (2–6), 898–903. https://doi.org/10.1016/j.radmeas.2007.12.032.

Beierholm, A.R., Behrens, C.F., Andersen, C.E., 2014. Dosimetric characterization of the Exradin W1 plastic scintillator detector through comparison with an in-house developed scintillator system. Radiat. Meas. 69, 50–56. https://doi.org/10.1016/j.radmeas.2014.08.005.

Beierholm, A.R., Lindvold, L.R., Andersen, C.E., 2011. Organic scintillators with long luminescent lifetimes for radiotherapy dosimetry. Radiat. Meas. 46 (12), 1982–1984. https://doi.org/10.1016/j.radmeas.2011.04.016.

Bertoldi, M., Green, D.R., Hagopian, V., Marraffino, J., Ronzhin, A., Thomaston, J., 1997. Section A Scintillators in magnetic fields up to 20 T. Nucl. Instrum. Methods Phys. Res. 386 (1997), 301–306. https://doi.org/10.1016/S0168-9002(96)01178-3.

Bielaiew, A.F., 1993. The effect of strong longitudinal magnetic fields on dose deposition from electron and photon beams. Med. Phys. 20 (4), 1171–1179. https://doi.org/10.1118/1.597149.

Birajdar, S., Zhang, W., Santos, A., Hickson, K., Afshar Vahid, S., 2023. Real-time *in vivo* dose measurement using ruby-based fibre optic dosimetry during internal radiation therapy. Phys. Eng. Sci. Med. 46 (3), 1205–1213. https://doi.org/10.1007/s13246-023-01288-7.

Birks, J.B., 1951. Scintillations from organic crystals: specific fluorescence and relative response to different radiations. Proc. Phys. Soc. 64 (10), 874. https://doi.org/10.1088/0370-1298/64/10/303.

Blömker, D., Holm, U., Klanner, R., Krebs, B., 1992. Plastic scintillators in magnetic fields. Nucl. Instrum. Methods Phys. Res. Sect. A Accel. Spectrom. Detect. Assoc. Equip. 311 (3), 505–511. https://doi.org/10.1016/0168-9002(92)90648-N.

Bouchard, H., Bielajew, A., 2015. Lorentz force correction to the Boltzmann radiation transport equation and its implications for Monte Carlo algorithms. Phys. Med. Biol. 60 (13), 4963–4971. https://doi.org/10.1088/0031-9155/60/13/4963.

Braccini, S., Ereditato, A., Giacoppo, F., Kreslo, I., Nesteruk, K.P., Nirkko, M., Weber, M., Scampoli, P., Neff, M., Pilz, S., Romano, V., 2012. A beam monitor detector based on doped silica and optical fibres. J. Instrum. 7 (2), T02001 https://doi.org/10.1088/1748-0221/7/02/T02001.

Bykov, T.A., Kasatov, D.A., Koshkarev, A.M., Makarov, A.N., Leonov, V.V., Porosev, V.V., Savinov, G.A., Savinov, S.S., Shchudlo, I.M., Taskaev, S.Y., Verkhovod, G.D., 2021. Evaluation of depth-dose profiles in a water phantom at the BNCT facility at BINP. J. Instrum. 16 (10) https://doi.org/10.1088/1748-0221/16/10/P10016.

Cantley, J.L., Cheng, C.W., Jesseph, F.B., Podder, T.K., Colussi, V.C., Traughber, B.J., Ponsky, L.E., Ellis, R.J., 2016. Real-time *in vivo* dosimetry for SBRT prostate treatment using plastic scintillating dosimetry embedded in a rectal balloon: a case study. J. Appl. Clin. Med. Phys. 17 (6), 305–311. https://doi.org/10.1120/jacmp.v17i6.6508.

Carrara, M., Tenconi, C., Guilizzoni, R., Borroni, M., Cavatorta, C., Cerrotta, A., Fallai, C., Gambarini, G., Vedda, A., Pignoli, E., 2014. Stem effect of a Ce3+ doped SiO2 optical dosimeter irradiated with a 192Ir HDR brachytherapy source. Radiat. Phys. Chem. 104, 175–179. https://doi.org/10.1016/j.radphyschem.2013.11.028.

Carrasco, P., Jornet, N., Jordi, O., Lizondo, M., Latorre-Musoll, A., Eudaldo, T., Ruiz, A., Ribas, M., 2015. Characterization of the Exradin W1 scintillator for use in radiotherapy. Med. Phys. 42 (1), 297–304. https://doi.org/10.1118/1.4903757.

Cecchi, D.D., Therriault-Proulx, F., Lambert-Girard, S., Hart, A., Macdonald, A., Pfleger, M., Lenckowski, M., Bazalova-Carter, M., 2021. Characterization of an x-ray tube-based ultrahigh dose-rate system for *in vitro* irradiations. Med. Phys. 48 (11), 7399–7409. https://doi.org/10.1002/mp.15234.

Cervantes, Y., Duane, S., Bouchard, H., 2022. Monte Carlo investigation of electron fluence perturbation in MRI-guided radiotherapy beams using six commercial radiation detectors. Phys. Med. Biol. 67 (3) https://doi.org/10.1088/1361-6560/ac4b36.

Cervantes, Y., Duchaine, J., Billas, I., Duane, S., Bouchard, H., 2021. Monte Carlo calculation of detector perturbation and quality correction factors in a 1.5 T magnetic resonance guided radiation therapy small photon beams. Phys. Med. Biol. 66 (22) https://doi.org/10.1088/1361-6560/ac3344.

Christensen, J.B., Almhagen, E., Stolarczyk, L., Vestergaard, A., Bassler, N., Andersen, C.E., 2019. Ionization quenching in scintillators used for dosimetry of mixed particle fields. Phys. Med. Biol. 64 (9), 095018 https://doi.org/10.1088/1361-6560/ab12f2.

Christensen, J.B., Vestergaard, A., Andersen, C.E., 2020. Using a small-core graphite calorimeter for dosimetry and scintillator quenching corrections in a therapeutic proton beam. Phys. Med. Biol. 65 (21), 215023 https://doi.org/10.1088/1361-6560/ab9bc3.

Clift, M.A., Johnston, P.N., Webb, D.V., 2002. A temporal method of avoiding the Cerenkov radiation generated in organic scintillator dosimeters by pulsed mega-voltage electron and photon beams. Phys. Med. Biol. 47 (8), 1421. https://doi.org/10.1088/0031-9155/47/8/313.

Clift, M.A., Sutton, R.A., Webb, D.V., 2000. Dealing with Cerenkov radiation generated in organic scintillator dosimeters by bremsstrahlung beams. Phys. Med. Biol. 45 (5), 1165–1182. https://doi.org/10.1088/0031-9155/45/5/307.

Cumalat, J.P., Cheung, H.W.K., Hassed, J., Smith, B.D., Bross, A.D., 1990. Effects of magnetic fields on the light yield of scintillators. Nucl. Instrum. Methods Phys. Res. Sect. A Accel. Spectrom. Detect. Assoc. Equip. 293 (3), 606–614. https://doi.org/10.1016/0168-9002(90)90331-Y.

Darafsheh, A., Taleei, R., Kassaee, A., Finlay, J.C., 2016. The visible signal responsible for proton therapy dosimetry using bare optical fibers is not Cerenkov radiation. Med. Phys. 43 (11), 5973–5980. https://doi.org/10.1118/1.4964453.

Darafsheh, A., Taleei, R., Kassaee, A., Finlay, J.C., 2017a. On the origin of the visible light responsible for proton dose measurement using plastic optical fibers. Des. Qual. Biomed. Technol. X 10056, 100560V. https://doi.org/10.1117/12.2252695.

Darafsheh, A., Taleei, R., Kassaee, A., Finlay, J.C., 2017b. Proton therapy dosimetry by using silica glass optical fiber microprobes. Opt. Fiber. Sens. Med. Diagnost. Treatment Appl. XVII 10058, 100580B. https://doi.org/10.1117/12.2252583.

Darafsheh, A., Taleei, R., Kassaee, A., Finlay, J.C., 2017c. Proton therapy dosimetry using the scintillation of the silica fibers. Opt Lett. 42 (4), 847. https://doi.org/10.1364/ol.42.000847.

Darafsheh, A., Zhang, R., Kassaee, A., Finlay, J.C., 2018. Characterization of the proton irradiation induced luminescence of materials and application in radiation oncology dosimetry. Proc. SPIE 10478, 1047815. https://doi.org/10.1117/12.2289315.

De Boer, S.F., Beddar, A.S., Rawlinson, J.A., 1993. Optical filtering and spectral measurements of radiation-induced light in plastic scintillation dosimetry. Phys. Med. Biol. 38 (7), 945. https://doi.org/10.1088/0031-9155/38/7/005.

de Freitas Nascimento, L., Leblans, P., van der Heyden, B., Akselrod, M., Goossens, J., Correa Rocha, L.E., Vaniqui, A., Verellen, D., 2022. Characterisation and quenching correction for an Al_2O_3:C optical fibre real time system in therapeutic proton, helium, and carbon-charged beams. Sensors 22 (23). https://doi.org/10.3390/s22239178.

De Pooter, J.A., De Prez, L.A., Bouchard, H., 2015. Application of an adapted Fano cavity test for Monte Carlo simulations in the presence of B-fields. Phys. Med. Biol. 60 (24), 9313–9327. https://doi.org/10.1088/0031-9155/60/24/9313.

Debnath, S.B.C., Tonneau, D., Fauquet, C., Tallet, A., Goncalves, A., Darreon, J., 2021. Dosimetric characterization of a small-scale (Zn,Cd)S:Ag inorganic scintillating detector to be used in radiotherapy. Phys. Med. 84, 15–23. https://doi.org/10.1016/j.ejmp.2021.03.022.

Di Martino, F., Barca, P., Barone, S., Bortoli, E., Borgheresi, R., De Stefano, S., Di Francesco, M., Grasso, L., Lucia, G., Linsalata, S., Marfisi, D., Pacitti, M., Migliorati, M., Felici, G., Palumbo, L., Faillace, L., 2020. FLASH radiotherapy with electrons: issues related to the production, monitoring, and dosimetric characterization of the beam. Front. Phys. 8 https://doi.org/10.3389/fphy.2020.570697.

Di Martino, F., Del Sarto, D., Giuseppina Bisogni, M., Capaccioli, S., Galante, F., Gasperini, A., Linsalata, S., Mariani, G., Pacitti, M., Paiar, F., Ursino, S., Vanreusel, V., Verellen, D., Felici, G., 2022. A new solution for UHDP and UHDR (Flash) measurements: theory and conceptual design of ALLS chamber. Phys. Med. 102, 9–18. https://doi.org/10.1016/j.ejmp.2022.08.010.

Dimitriadis, A., Patallo, I.S., Billas, I., Duane, S., Nisbet, A., Clark, C.H., 2017. Characterisation of a plastic scintillation detector to be used in a multicentre stereotactic radiosurgery dosimetry audit. Radiat. Phys. Chem. 140, 373–378. https://doi.org/10.1016/j.radphyschem.2017.02.023.

Ding, L., Wu, Q., Wang, Q., Li, Y., Perks, R.M., Zhao, L., 2020. Advances on inorganic scintillator-based optic fiber dosimeters. Issue 1. In: EJNMMI Physics, vol. 7. Springer Science and Business Media Deutschland GmbH. https://doi.org/10.1186/s40658-020-00327-6.

Eichmann, M., Thomann, B., 2017. Air core detectors for Cerenkov-free scintillation dosimetry of brachytherapy β-sources. Med. Phys. 44 (9), 4900–4909. https://doi.org/10.1002/mp.12374.

Esplen, N., Mendonca, M.S., Bazalova-Carter, M., 2020. Physics and biology of ultrahigh dose-rate (FLASH) radiotherapy: a topical review, 23. In: Physics in Medicine and Biology, vol. 65. IOP Publishing Ltd. https://doi.org/10.1088/1361-6560/abaa28.

Esposito, M., Villaggi, E., Bresciani, S., Cilla, S., Falco, M.D., Garibaldi, C., Russo, S., Talamonti, C., Stasi, M., Mancosu, P., 2020. Estimating dose delivery accuracy in stereotactic body radiation therapy: a review of in-vivo measurement methods. In: Radiotherapy and Oncology, vol. 149. Elsevier Ireland Ltd, pp. 158–167. https://doi.org/10.1016/j.radonc.2020.05.014.

Fallone, B.G., 2014. The rotating biplanar linac-magnetic resonance imaging system. Issue 3. In: Seminars in Radiation Oncology, vol. 24, pp. 200–202. https://doi.org/10.1016/j.semradonc.2014.02.011. W.B. Saunders.

Favaudon, V., Caplier, L., Monceau, V., Pouzoulet, F., Sayarath, M., Fouillade, C., Poupon, M.-F., Brito, I., Hupé, P., Bourhis, J., Hall, J., Fontaine, J.-J., Vozenin, M.-C., 2014. Ultrahigh dose-rate FLASH irradiation increases the differential response between normal and tumor tissue in mice, 2014 Jul 16 Sci. Transl. Med. 6 (245), 245ra93. https://doi.org/10.1126/scitranslmed.3008973.

Ferrer, C., Huertas, C., García, D., Sáez, M., 2023. Dosimetric characterization of a novel commercial plastic scintillation detector with an MR-Linac. Med. Phys. 50 (4), 2525–2539. https://doi.org/10.1002/mp.16204.

Fonseca, G.P., Johansen, J.G., Smith, R.L., Beaulieu, L., Beddar, S., Kertzscher, G., Verhaegen, F., Tanderup, K., 2020. *In vivo* dosimetry in brachytherapy: requirements and future directions for research, development, and clinical practice. In: Physics and Imaging in Radiation Oncology, vol. 16. Elsevier Ireland Ltd, pp. 1–11. https://doi.org/10.1016/j.phro.2020.09.002.

Fontbonne, J.M., Iltis, G., Ban, G., Battala, A., Vernhes, J.C., Tillier, J., Bellaize, N., Le Brun, C., Tamain, B., Mercier, K., Motin, J.C., 2002. Scintillating fiber dosimeter for radiation therapy accelerator. IEEE Trans. Nucl. Sci. 49 I (5), 2223–2227. https://doi.org/10.1109/TNS.2002.803680.

Francescon, P., Beddar, S., Satariano, N., Das, I.J., 2014. Variation of kQclin, Qmsr fclin, fmsr for the small-field dosimetric parameters percentage depth dose, tissue-maximum ratio, and off-axis ratio. Med. Phys. 41 (10) https://doi.org/10.1118/1.4895978.

Frelin, A.M., Fontbonne, J.M., Ban, G., Colin, J., Labalme, M., Batalla, A., Isambert, A., Vela, A., Leroux, T., 2005. Spectral discrimination of Čerenkov radiation in scintillating dosimeters. Med. Phys. 32 (9), 3000–3006. https://doi.org/10.1118/1.2008487.

Gagnon, J.C., Thériault, D., Guillot, M., Archambault, L., Beddar, S., Gingras, L., Beaulieu, L., 2012. Dosimetric performance and array assessment of plastic scintillation detectors for stereotactic radiosurgery quality assurance. Med. Phys. 39 (1), 429–436. https://doi.org/10.1118/1.3666765.

Galavis, P.E., Hu, L., Holmes, S., Das, I.J., 2019. Characterization of the plastic scintillation detector Exradin W2 for small field dosimetry. Med. Phys. 46 (5), 2468–2476. https://doi.org/10.1002/mp.13501.

Gao, Y., Liu, R., Chang, C.W., Charyyev, S., Zhou, J., Bradley, J.D., Liu, T., Yang, X., 2022. A potential revolution in cancer treatment: a topical review of FLASH radiotherapy. Issue 10. In: Journal of Applied Clinical Medical Physics, vol. 23. John Wiley and Sons Ltd. https://doi.org/10.1002/acm2.13790.

Gargett, M., Oborn, B., Metcalfe, P., Rosenfeld, A., 2015. Monte Carlo simulation of the dose response of a novel 2D silicon diode array for use in hybrid MRI-LINAC systems. Med. Phys. 42 (2), 856–865. https://doi.org/10.1118/1.4905108.

Gaza, R., McKeever, S.W.S., 2006. A real-time, high-resolution optical fibre dosemeter based on optically stimulated luminescence (OSL) of KBr:Eu, for potential use during the radiotherapy of cancer. Radiat. Protect. Dosim. 120 (1–4), 14–19. https://doi.org/10.1093/rpd/nci603.

Gaza, R., McKeever, S.W.S., Akselrod, M.S., 2005. Near-real-time radiotherapy dosimetry using optically stimulated luminescence of Al2O3:C: mathematical models and preliminary results. Med. Phys. 32 (4), 1094–1102. https://doi.org/10.1118/1.1884365.

Gaza, R., McKeever, S.W.S., Akselrod, M.S., Akselrod, A., Underwood, T., Yoder, C., Andersen, C.E., Aznar, M.C., Marckmann, C.J., Bøtter-Jensen, L., 2004. A fiber-dosimetry method based on OSL from Al2O3:C for radiotherapy applications. Radiat. Meas. 38 (4–6), 809–812. https://doi.org/10.1016/j.radmeas.2003.12.004.

Gingras, L., Côté, B., Berthiaume, F., Lambert-Girard, S., Leblanc, D., Archambault, L., Beaulieu, L., Therriault-Proulx, F., 2021. Small field dosimetry of a Varian TrueBeam High Definition MLC linear accelerator using the Hyperscint RP200 scintillation detector. COMP Ann. Scient. Meet. 2021, 6C – 6.

Girard, S., Francesca, D. Di, Morana, A., Hoehr, C., Paillet, P., Duzenli, C., Kerboub, N., Reghioua, I., Vecchi, G.L., Alessi, A., Duhamel, O., Trinczek, M., Marin, E., Boukenter, A., Ouerdane, Y., Mekki, J., Alia, R.G., Kadi, Y., Brugger, M., 2019. X-rays, γ -rays, and proton beam monitoring with multimode nitrogen-doped optical fiber. IEEE Trans. Nucl. Sci. 66 (1), 306–311. https://doi.org/10.1109/TNS.2018.2879791.

Gómez, F., Gonzalez-Castaño, D.M., Fernández, N.G., Pardo-Montero, J., Schüller, A., Gasparini, A., Vanreusel, V., Verellen, D., Felici, G., Kranzer, R., Paz-Martín, J., 2022. Development of an ultra-thin parallel plate ionization chamber for dosimetry in FLASH radiotherapy. Med. Phys. 49 (7), 4705–4714. https://doi.org/10.1002/mp.15668.

Grotzer, M.A., Schültke, E., Bräuer-Krisch, E., Laissue, J.A., 2015. Microbeam radiation therapy: clinical perspectives. Phys. Med. 31 (6), 564–567. https://doi.org/10.1016/j.ejmp.2015.02.011.

Guillot, M., Gingras, L., Archambault, L., Beddar, S., Beaulieu, L., 2011. Spectral method for the correction of the Cerenkov light effect in plastic scintillation detectors: a comparison study of calibration procedures and validation in Cerenkov light-dominated situations. Med. Phys. 38 (4), 2140–2150. https://doi.org/10.1118/1.3562896.

Hart, A., Cecchi, D., Giguère, C., Larose, F., Therriault-Proulx, F., Esplen, N., Beaulieu, L., Bazalova-Carter, M., 2022. Lead-doped scintillator dosimeters for detection of ultrahigh dose-rate x-rays. Phys. Med. Biol. 67 (10) https://doi.org/10.1088/1361-6560/ac69a5.

Helo, Y., Kacperek, A., Rosenberg, I., Royle, G., Gibson, A.P., 2014. The physics of Cerenkov light production during proton therapy. Phys. Med. Biol. 59 (23), 7107–7123. https://doi.org/10.1088/0031-9155/59/23/7107.

Herreros, A., Pérez-Calatayud, J., Ballester, F., Barrera-Gómez, J., Abellana, R., Melo, J., Moutinho, L., Tagliaferri, L., Rovirosa, Á., 2022. *In vivo* verification of treatment source dwell times in brachytherapy of postoperative endometrial carcinoma: a feasibility study. J. Personalized Med. 12 (6) https://doi.org/10.3390/jpm12060911.

Hoehr, C., Hanna, M., Zeisler, S., Penner, C., Stokely, M., Dehnel, M., 2020. Ce-and B-doped silica fibers for monitoring Low-energy proton beams on a medical cyclotron. Appl. Sci. 10 (13) https://doi.org/10.3390/app10134488.

Hoehr, C., Lindsay, C., Beaudry, J., Penner, C., Strgar, V., Lee, R., Duzenli, C., 2018. Characterization of the exradin W1 plastic scintillation detector for small field applications in proton therapy. Phys. Med. Biol. 63 (9), 095016 https://doi.org/10.1088/1361-6560/aabd2d.

Hoehr, C., Morana, A., Duhamel, O., Capoen, B., Trinczek, M., Paillet, P., Duzenli, C., Bouazaoui, M., Bouwmans, G., Cassez, A., Ouerdane, Y., Boukenter, A., El Hamzaoui, H., Girard, S., 2019. Novel Gd3+-doped silica-based optical fiber material for dosimetry in proton therapy. Sci. Rep. 9 (1) https://doi.org/10.1038/s41598-019-52608-5.

Huang, C.-Y., Yang, B., Lam, W.W., Geng, H., Cheung, K.Y., Yu, S.K., 2023. Magnetic field induced dose effects in radiation therapy using MR-linacs. Med. Phys. 50 (6), 3623–3636. https://doi.org/10.1002/mp.16397.

International Atomic Energy Agency, 2017. Dosimetry of small static fields used in external beam radiotherapy. Technical Report Series No. 483. https://www.iaea.org/publications/11075/dosimetry-of-small-static-fields-used-in-external-beam-radiotherapy. (Accessed 12 January 2024).

Ishikawa, M., Nagase, N., Matsuura, T., Hiratsuka, J., Suzuki, R., Miyamoto, N., Sutherland, K.L., Fujita, K., Shirato, H., 2015. Development of a wavelength-separated type scintillator with optical fiber (SOF) dosimeter to compensate for the Cerenkov radiation effect. J. Radiat. Res. 56 (2), 372–381. https://doi.org/10.1093/jrr/rru106.

Jacqmin, D.J., Miller, J.R., Barraclough, B.A., Labby, Z.E., 2022. Commissioning an Exradin W2 plastic scintillation detector for clinical use in small radiation fields. J. Appl. Clin. Med. Phys. 23 (8) https://doi.org/10.1002/acm2.13728.

Jelley, J.V., 1955. Cerenkov radiation and its applications. Br. J. Appl. Phys. 6 (7), 227. https://doi.org/10.1088/0508-3443/6/7/301.

Jin, W.H., Seldon, C., Butkus, M., Sauerwein, W., Giap, H.B., 2022. A review of boron neutron capture therapy: its history and current challenges. Int. J. Part. Ther. 9 (1), 71–82. https://doi.org/10.14338/ijpt-22-00002.1.

Johansen, J.G., Kertzscher, G., Jørgensen, E.B., Rylander, S., Bentzen, L., Hokland, S.B., Søndergaard, C.S., With, A.K.M., Buus, S., Tanderup, K., 2019. Dwell time verification in brachytherapy based on time resolved *in vivo* dosimetry. Phys. Med. 60, 156–161. https://doi.org/10.1016/j.ejmp.2019.03.031.

Jordan, K.J., 1996. Evaluation of ruby as a fluorescent sensor for optical fiber-based radiation dosimetry. Proc. SPIE 2705, 170–178. https://doi.org/10.1117/12.236190.

Jørgensen, E.B., Kertzscher, G., Buus, S., Bentzen, L., Hokland, S.B., Rylander, S., Tanderup, K., Johansen, J.G., 2021. Accuracy of an *in vivo* dosimetry-based source tracking method for afterloading brachytherapy — a phantom study. Med. Phys. 48 (5), 2614–2623. https://doi.org/10.1002/mp.14812.

Justus, B.L., Falkenstein, P., Huston, A.L., Plazas, M.C., Ning, H., Miller, R.W., 2006. Elimination of Cerenkov interference in a fibre-optic-coupled radiation dosemeter. Radiat. Protect. Dosim. 120 (1–4), 20–23. https://doi.org/10.1093/rpd/nci525.

Kamio, Y., Bouchard, H., 2014. Correction-less dosimetry of nonstandard photon fields: a new criterion to determine the usability of radiation detectors. Phys. Med. Biol. 59 (17), 4973–5002. https://doi.org/10.1088/0031-9155/59/17/4973.

Kanouta, E., Johansen, J.G., Kertzscher, G., Sitarz, M.K., Sørensen, B.S., Poulsen, P.R., 2022. Time structure of pencil beam scanning proton FLASH beams measured with scintillator detectors and compared with log files. Med. Phys. 49 (3), 1932–1943. https://doi.org/10.1002/mp.15486.

Kanouta, E., Poulsen, P.R., Kertzscher, G., Sitarz, M.K., Sørensen, B.S., Johansen, J.G., 2023. Time-resolved dose rate measurements in pencil beam scanning proton FLASH therapy with a fiber-coupled scintillator detector system. Med. Phys. 50 (4), 2450–2462. https://doi.org/10.1002/mp.16156.

Keall, P.J., Barton, M., Crozier, S., 2014. The Australian magnetic resonance imaging-linac program. Semin. Radiat. Oncol. 24 (3), 203–206. https://doi.org/10.1016/j.semradonc.2014.02.015. W.B. Saunders.

Kelleter, L., Jolly, S., 2020. A mathematical expression for depth-light curves of therapeutic proton beams in a quenching scintillator. Med. Phys. 47 (5), 2300–2308. https://doi.org/10.1002/mp.14099.

Kertzscher, G., Beddar, S., 2016. Ruby-based inorganic scintillation detectors for 192Ir brachytherapy. Phys. Med. Biol. 61 (21), 7744–7764. https://doi.org/10.1088/0031-9155/61/21/7744.

Kertzscher, G., Beddar, S., 2019. Inorganic scintillation detectors for 192Ir brachytherapy. Phys. Med. Biol. 64 (22) https://doi.org/10.1088/1361-6560/ab421f.

Kertzscher, G., Andersen, C.E., Tanderup, K., 2014. Adaptive error detection for HDR/PDR brachytherapy: guidance for decision making during real-time *in vivo* point dosimetry. Med. Phys. 41 (5) https://doi.org/10.1118/1.4870438.

Kertzscher, G., Andersen, C.E., Edmund, J.M., Tanderup, K., 2011. Stem signal suppression in fiber-coupled Al2O3:C dosimetry for 192Ir brachytherapy. Radiat. Meas. 46 (12), 2020–2024. https://doi.org/10.1016/j.radmeas.2011.05.079.

Keyvanloo, A., Burke, B., Warkentin, B., Tadic, T., Rathee, S., Kirkby, C., Santos, D.M., Fallone, B.G., 2012. Skin dose in longitudinal and transverse linac-MRIs using Monte Carlo and realistic 3D MRI field models. Med. Phys. 39 (10), 6509–6521. https://doi.org/10.1118/1.4754657.

Kim, T.J., Cheng, K., Zhang, H., Liu, S., Skinner, L., Xing, L., 2020. Second window near-infrared dosimeter (NIR2D) system for radiation dosimetry. Phys. Med. Biol. 65 (17) https://doi.org/10.1088/1361-6560/ab9b56.

Klavsen, M.F., Ankjærgaard, C., Behrens, C.P., Vogelius, I.R., Boye, K., Hansen, R.H., Andersen, C.E., 2022. Time-resolved plastic scintillator dosimetry in MR linear accelerators without image distortion. Radiat. Meas. 154 https://doi.org/10.1016/j.radmeas.2022.106759.

Klein, D.M., McKeever, S.W.S., 2008. Optically stimulated luminescence from KBr:Eu as a near-real-time dosimetry system. Radiat. Meas. 43 (2–6), 883–887. https://doi.org/10.1016/j.radmeas.2008.01.015.

Klein, D., Peakheart, D.W., McKeever, S.W.S., 2010. Performance of a near-real-time KBr:Eu dosimetry system under computed tomography x-rays. Radiat. Meas. 45 (3–6), 663–667. https://doi.org/10.1016/j.radmeas.2009.11.043.

Klein, F.A., Greilich, S., Andersen, C.E., Lindvold, L.R., Jäkel, O., 2011. A thin layer fiber-coupled luminescence dosimeter based on Al2O3:C. Radiat. Meas. 46 (12), 1607–1609. https://doi.org/10.1016/j.radmeas.2011.05.030.

Lagendijk, J.J.W., Raaymakers, B.W., van Vulpen, M., 2014. The magnetic resonance imaging-linac system. Issue 3. In: Seminars in Radiation Oncology, vol. 24, pp. 207–209. https://doi.org/10.1016/j.semradonc.2014.02.009. W.B. Saunders.

Lambert, J., Yin, Y., McKenzie, D.R., Law, S.H., Ralston, A., Suchowerska, N., 2010. A prototype scintillation dosimeter customized for small and dynamic megavoltage radiation fields. Phys. Med. Biol. 55 (4), 1115–1126. https://doi.org/10.1088/0031-9155/55/4/014.

Lambert, J., Yin, Y., McKenzie, D.R., Law, S., Suchowerska, N., 2008. Cerenkov-free scintillation dosimetry in external beam radiotherapy with an air core light guide. Phys. Med. Biol. 53 (11), 3071–3080. https://doi.org/10.1088/0031-9155/53/11/021.

Le Deroff, C., Pérès, E.A., Ledoux, X., Toutain, J., Frelin-Labalme, A.M., 2020. *In vivo* surface dosimetry with a scintillating fiber dosimeter in preclinical image-guided radiotherapy. Med. Phys. 47 (1), 234–241. https://doi.org/10.1002/mp.13903.

Lebel-Cormier, M.A., Boilard, T., Bernier, M., Beaulieu, L., 2021. Medical range radiation dosimeter based on polymer-embedded fiber bragg gratings. Sensors 21 (23). https://doi.org/10.3390/s21238139.

Lee, B., Jang, K.W., Cho, D.H., Yoo, W.J., Tack, G.R., Chung, S.C., Kim, S., Cho, H., 2007. Measurements and elimination of Cherenkov light in fiber-optic scintillating detector for electron beam therapy dosimetry. Nucl. Instrum. Methods Phys. Res. Sect. A Accel. Spectrom. Detect. Assoc. Equip. 579 (1), 344–348. https://doi.org/10.1016/j.nima.2007.04.074.

Lee, J.J., Liu, P.Z., McKenzie, D.R., Suchowerska, N., 2013. A method to remove residual signals in fibre optic luminescence dosimeters. Phys. Med. Biol. 58 (5), 1581–1590. https://doi.org/10.1088/0031-9155/58/5/1581.

Lee, S., Hong, B., Lee, K.S., Mulilo, B., Keun Park, S., 2013. Construction and performance of a dose-verification scintillation-fiber detector for proton therapy. Nucl. Instrum. Methods Phys. Res. Sect. A Accel. Spectrom. Detect. Assoc. Equip. 724, 6–11. https://doi.org/10.1016/j.nima.2013.05.053.

Létourneau, D., Pouliot, J., Roy, R., 1999. Miniature scintillating detector for small field radiation therapy. Med. Phys. 26 (12), 2555–2561. https://doi.org/10.1118/1.598793.

Linares Rosales, H.M., Johansen, J.G., Kertzscher, G., Tanderup, K., Beaulieu, L., Beddar, S., 2021. 3D source tracking and error detection in HDR using two independent scintillator dosimetry systems. Med. Phys. 48 (5), 2095–2107. https://doi.org/10.1002/mp.14607.

Liu, P.Z.Y., Suchowerska, N., McKenzie, D.R., 2013. Twisted pair of optic fibers for background removal in radiation fields. Appl. Opt. 52 (22), 5500–5507. https://doi.org/10.1364/AO.52.005500.

Liu, P.Z.Y., Suchowerska, N., Lambert, J., Abolfathi, P., McKenzie, D.R., 2011. Plastic scintillation dosimetry: comparison of three solutions for the Cerenkov challenge. Phys. Med. Biol. 56 (18), 5805–5821. https://doi.org/10.1088/0031-9155/56/18/003.

Lo Presti, D., Bonanno, D.L., Longhitano, F., Bongiovanni, D.G., Russo, G.V., Leonora, E., Randazzo, N., Reito, S., Sipala, V., Gallo, G., 2016. Design and characterisation of a real time proton and carbon ion radiography system based on scintillating optical fibres. Phys. Med. 32 (9), 1124–1134. https://doi.org/10.1016/j.ejmp.2016.08.015.

Looe, H.K., Delfs, B., Poppinga, D., Harder, D., Poppe, B., 2017. Magnetic field influences on the lateral dose response functions of photon-beam detectors: MC study of wall-less water-filled detectors with various densities. Phys. Med. Biol. 62 (12), 5131–5148. https://doi.org/10.1088/1361-6560/aa6ca0.

Madden, L., 2022. In: Optical Dosimeters for Radiotherapy with MRI-LINACs. University of Wollongong Thesis Collections 2017+. https://ro.uow.edu.au/theses1. (Accessed 12 January 2024).

Madden, L., Archer, J., Li, E., Jelen, U., Dong, B., Holloway, L., Rosenfeld, A., 2020. MRI-LINAC beam profile measurements using a plastic scintillation dosimeter. Phys. Med. 73, 111–116. https://doi.org/10.1016/j.ejmp.2020.04.016.

Madden, L., Archer, J., Li, E., Jelen, U., Dong, B., Roberts, N., Holloway, L., Rosenfeld, A., 2019. First measurements with a plastic scintillation dosimeter at the Australian MRI-LINAC. Phys. Med. Biol. 64 (17) https://doi.org/10.1088/1361-6560/ab324b.

Madden, L., Archer, J., Li, E., Wilkinson, D., Rosenfeld, A., 2018b. Temporal separation of Cerenkov radiation and scintillation using a clinical LINAC and artificial intelligence. Phys. Med. Biol. 63 (22) https://doi.org/10.1088/1361-6560/aae938.

Madden, L., Archer, J., Li, E., Wilkinson, D., Rosenfeld, A., 2018a. Temporal separation of Cerenkov radiation and scintillation using artificial neural networks in Clinical LINACs. Phys. Med. 54, 131–136. https://doi.org/10.1016/j.ejmp.2018.10.007.

Madden, L., Holloway, L., Rosenfeld, A., Li, E., 2022. Fibre-optic dosimetry for MRI-LINACs: a mini-review. In: Frontiers in Physics, vol. 10. Frontiers Media SA. https://doi.org/10.3389/fphy.2022.879624.

Madden, L., Lukas, E., Santos, A., Ganija, M., Veitch, P., Rosenfeld, A., Li, E., 2021a. Deconvolution analysis improves real-time OSL of BeO ceramic. Radiat. Meas. 149, 106680 https://doi.org/10.1016/j.radmeas.2021.106680.

Madden, L., Roberts, N., Jelen, U., Dong, B., Holloway, L., Metcalfe, P., Rosenfeld, A., Li, E., 2021b. In-line MRI-LINAC depth dose measurements using an in-house plastic scintillation dosimeter. Biomed. Phys. Eng. Exp. 7 (2) https://doi.org/10.1088/2057-1976/abe295.

Magne, S., Deloule, S., Ostrowsky, A., Ferdinand, P., 2013. Fiber-coupled, time-gated Al2O3: C radioluminescence dosimetry technique and algorithm for radiation therapy with LINACs. IEEE Trans. Nucl. Sci. 60 (4), 2998–3007. https://doi.org/10.1109/TNS.2013.2263640.

Marckmann, C.J., Aznar, M.C., Andersen, C.E., Bøtter-Jensen, L., 2006. Influence of the stem effect on radioluminescence signals from optical fibre Al2O3:C dosemeters. Radiat. Protect. Dosim. 119 (1–4), 363–367. https://doi.org/10.1093/rpd/nci507.

Marinelli, M., Felici, G., Galante, F., Gasparini, A., Giuliano, L., Heinrich, S., Pacitti, M., Prestopino, G., Vanreusel, V., Verellen, D., Verona, C., Verona Rinati, G., 2022. Design, realization, and characterization of a novel diamond detector prototype for FLASH radiotherapy dosimetry. Med. Phys. 49 (3), 1902–1910. https://doi.org/10.1002/mp.15473.

Martínez, N., Rucci, A., Marcazzó, J., Molina, P., Santiago, M., Cravero, W., 2017. Characterization of YVO4:Eu3+ scintillator as detector for fiber optic dosimetry. Radiat. Meas. 106, 650–656. https://doi.org/10.1016/j.radmeas.2017.03.015.

Martinez, N., Teichmann, T., Molina, P., Sommer, M., Santiago, M., Henniger, J., Caselli, E., 2015. Scintillation properties of the YVO4: Eu3+ compound in powder form: its application to dosimetry in radiation fields produced by pulsed mega-voltage photon beams. Zeitschrift Fur Medizinische Physik 25 (4), 368–374. https://doi.org/10.1016/j.zemedi.2015.04.001.

Martyn, M., Kam, W., Woulfe, P., O'Keeffe, S., 2023. Water phantom characterization of a novel optical fiber sensor for LDR brachytherapy. IEEE Sensor. J. 23 (2), 1146–1156. https://doi.org/10.1109/JSEN.2022.3225007.

Mattei, I., Battistoni, G., De Simoni, M., Dong, Y., Embriaco, A., Fischetti, M., Giacometti, V., Gioscio, E., Magi, M., Mancini-Terracciano, C., Marafini, M., Mirabelli, R., Muraro, S., Sarti, A., Sciubba, A., Camillocci, E.S., Toppi, M., Traini, G., Valle, S.M., Patera, V., 2018. Scintillating fiber devices for particle therapy applications. IEEE Trans. Nucl. Sci. 65 (8), 2054–2060. https://doi.org/10.1109/TNS.2018.2843179.

Mattei, I., Battistoni, G., De Simoni, M., Dong, Y., Embriaco, A., Fischetti, M., Gioscio, E., Mancini-Terracciano, C., Marafini, M., Mirabelli, R., Muraro, S., Sarti, A., Sciubba, A., Solfaroli Camillocci, E., Traini, G., Valle, S.M., Patera, V., 2020. Charged particles and neutron trackers: applications to particle therapy. In: Nuclear Instruments and Methods in Physics Research, Section A: Accelerators, Spectrometers, Detectors and Associated Equipment, vol. 954. Elsevier B.V. https://doi.org/10.1016/j.nima.2018.09.064

McKeever, S.W.S., 2011. Optically stimulated luminescence: a brief overview. Radiat. Meas. 46 (12), 1336–1341. https://doi.org/10.1016/j.radmeas.2011.02.016.

McKeever, S.W.S., Sholom, S., Shrestha, N., Klein, D.M., 2020. An in-situ, fiber-optic system for sub-surface, environmental dose measurements using radiophotoluminescence from Ag-doped alkali-phosphate glass. Radiat. Meas. 132 https://doi.org/10.1016/j.radmeas.2020.106273.

Metzner, E., Bäumer, C., Behrends, C., Dammene Debbih, A., Döhler, D.D., van Goethem, M.J., van der Graaf, E.R., Kahle, P., Lühr, A., Teichmann, T., Timmermann, B., Weinberger, D., Werner, T., Wulff, J., Kormoll, T., 2022. Spectral fiber dosimetry with beryllium oxide for quality assurance in hadron radiation therapy. J. Instrum. 17 (2), P02009 https://doi.org/10.1088/1748-0221/17/02/P02009.

Mijnheer, B., Beddar, S., Izewska, J., Reft, C., 2013. *In vivo* dosimetry in external beam radiotherapy. Med. Phys. 40 (7) https://doi.org/10.1118/1.4811216.

Molina, P., Santiago, M., Marcazzó, J., Spano, F., Henniger, J., Cravero, W., Caselli, E., 2012. Radioluminescence of red-emitting Eu-doped phosphors for fiberoptic dosimetry. Appl. Radiat. Isot. 71 (Suppl. L), 12–14. https://doi.org/10.1016/j.apradiso.2012.01.005.

Molina, P., Sommer, M., Kattner, F., Henniger, J., 2013. Response characterization of an Y2O3:Eu-based radioluminescence probe under 60Co irradiation. Radiat. Meas. 56, 338–341. https://doi.org/10.1016/j.radmeas.2013.01.031.

Mones, E., Veronese, I., Vedda, A., Loi, G., Fasoli, M., Moretti, F., Chiodini, N., Cannillo, B., Brambilla, M., 2008. Ce-doped optical fibre as radioluminescent dosimeter in radiotherapy. Radiat. Meas. 43 (2–6) https://doi.org/10.1016/j.radmeas.2008.01.031.

Morin, J., Béliveau-Nadeau, D., Chung, E., Seuntjens, J., Thériault, D., Archambault, L., Beddar, S., Beaulieu, L., 2013. A comparative study of small field total scatter factors and dose profiles using plastic scintillation detectors and other stereotactic dosimeters: the case of the CyberKnife. Med. Phys. 40 (1) https://doi.org/10.1118/1.4772190.

Morrocchi, M., Pensavalle, J.H., Ciarrocchi, E., Di Martino, F., Felici, G., Galante, F., Gasparini, A., Grasso, L., Linsalata, S., Massa, M., Moggi, A., Pacitti, M., Vanreusel, V., Verellen, D., Bisogni, M.G., 2022. Experimental characterization and Monte Carlo simulation of scintillator detectors in online electron FLASH radiotherapy dosimetry. J. Instrum. 17 (9) https://doi.org/10.1088/1748-0221/17/09/P09005.

Mutic, S., Dempsey, J.F., 2014. The ViewRay system: magnetic resonance-guided and controlled radiotherapy. Issue 3. In: Seminars in Radiation Oncology, vol. 24, pp. 196–199. https://doi.org/10.1016/j.semradonc.2014.02.008. W.B. Saunders.

Nascimento, L.F., Vanhavere, F., Kodaira, S., Kitamura, H., Verellen, D., De Deene, Y., 2015. Application of Al2O3:C+fibre dosimeters for 290MeV/n carbon therapeutic beam dosimetry. Radiat. Phys. Chem. 115, 75–80. https://doi.org/10.1016/j.radphyschem.2015.06.001.

Nascimento, L.F., Veronese, I., Loi, G., Mones, E., Vanhavere, F., Verellen, D., 2018. Radioluminescence results from an Al_2O_3:C fiber prototype: 6 MV medical beam. Sens. Actuators, A 274. https://doi.org/10.1016/j.sna.2018.03.007.

O'Keeffe, S., Fitzpatrick, C., Lewis, E., Al-Shamma'a, A.I., 2008. A review of optical fibre radiation dosimeters. Sens. Rev. 28 (2), 136–142. https://doi.org/10.1108/02602280810856705.

Oborn, B.M., Ge, Y., Hardcastle, N., Metcalfe, P.E., Keall, P.J., 2016. Dose enhancement in radiotherapy of small lung tumors using inline magnetic fields: a Monte Carlo based planning study. Med. Phys. 43 (1), 368–377. https://doi.org/10.1118/1.4938580.

Oborn, B.M., Metcalfe, P.E., Butson, M.J., Rosenfeld, A.B., Keall, P.J., 2012. Electron contamination modeling and skin dose in 6 MV longitudinal field MRIgRT: impact of the MRI and MRI fringe field. Med. Phys. 39 (2), 874–890. https://doi.org/10.1118/1.3676181.

Okamura, K., Akino, Y., Inoue, S., Isohashi, F., Seo, Y., Tamari, K., Hirata, T., Hayashi, K., Fumimoto, Y., Ogawa, K., 2022. Evaluation of calibration methods of Exradin W2 plastic scintillation detector for CyberKnife small-field dosimetry. Radiat. Meas. 156 https://doi.org/10.1016/j.radmeas.2022.106821.

Olusoji, O.J., Penner, C., Bélanger-Champagne, C., Kam, W., Martyn, M., Woulfe, P., Hoehr, C., O'keeffe, S., 2021. Dosimetric application of phosphorus doped fibre for x-ray and proton therapy. Sensors 21 (15). https://doi.org/10.3390/s21155157.

Papaconstadopoulos, P., Archambault, L., Seuntjens, J., 2017. Experimental investigation on the accuracy of plastic scintillators and of the spectrum discrimination method in small photon fields. Med. Phys. 44 (2), 654–664. https://doi.org/10.1002/mp.12064.

Papaconstadopoulos, P., Tessier, F., Seuntjens, J., 2014. On the correction, perturbation and modification of small field detectors in relative dosimetry. Phys. Med. Biol. 59 (19), 5937–5952. https://doi.org/10.1088/0031-9155/59/19/5937.

Particle Therapy Co-Operative Group Website:https://www.ptcog.site, last access: 12 January 2024.

Penner, C., Hoehr, C., O'Keeffe, S., Woulfe, P., Duzenli, C., 2018. Characterization of a terbium-activated gadolinium oxysulfide plastic optical fiber sensor in photons and protons. IEEE Sensor. J. 18 (4), 1513–1519. https://doi.org/10.1109/JSEN.2017.2780163.

Penner, C., Usherovich, S., Niedermeier, J., Belanger-Champagne, C., Trinczek, M., Paulssen, E., Hoehr, C., 2023. Organic scintillator-fibre sensors for proton therapy dosimetry: SCSF-3HF and EJ-260. Electronics (Switzerland) 12 (1). https://doi.org/10.3390/electronics12010011.

Poirier, Y., Xu, J., Mossahebi, S., Therriault-Proulx, F., Sawant, A., 2022. Technical note: characterization and practical applications of a novel plastic scintillator for online dosimetry for an ultrahigh dose rate (FLASH). Med. Phys. 49 (7), 4682–4692. https://doi.org/10.1002/mp.15671.

Polf, J.C., Yukihara, E.G., Akselrod, M.S., McKeever, S.W.S., 2004. Real-time luminescence from Al2O3 fiber dosimeters. Radiat. Meas. 38 (2), 227–240. https://doi.org/10.1016/j.radmeas.2003.10.005.

Raaijmakers, A.J.E., Raaymakers, B.W., Lagendijk, J.J.W., 2005. Integrating a MRI scanner with a 6 MV radiotherapy accelerator: dose increase at tissue-air interfaces in a lateral magnetic field due to returning electrons. Phys. Med. Biol. 50 (7), 1363–1376. https://doi.org/10.1088/0031-9155/50/7/002.

Raaymakers, B.W., Raaijmakers, A.J.E., Kotte, A.N.T.J., Jette, D., Lagendijk, J.J.W., 2004. Integrating a MRI scanner with a 6 MV radiotherapy accelerator: dose deposition in a transverse magnetic field. Phys. Med. Biol. 49 (17), 4109–4118. https://doi.org/10.1088/0031-9155/49/17/019.

Ralston, A., Liu, P., Warrener, K., McKenzie, D., Suchowerska, N., 2012. Small field diode correction factors derived using an air core fibre optic scintillation dosimeter and EBT2 film. Phys. Med. Biol. 57 (9), 2587–2602. https://doi.org/10.1088/0031-9155/57/9/2587.

Ramírez, M., Martínez, N., Marcazzó, J., Molina, P., Feld, D., Santiago, M., 2016. Performance of ZnSe(Te) as fiberoptic dosimetry detector. Appl. Radiat. Isot. 116, 1–7. https://doi.org/10.1016/j.apradiso.2016.07.007.

Romano, F., Bailat, C., Jorge, P.G., Lerch, M.L.F., Darafsheh, A., 2022. Ultra-high dose rate dosimetry: challenges and opportunities for FLASH radiation therapy. Med. Phys. 49 (7), 4912–4932. https://doi.org/10.1002/mp.15649.

Rossi, S., 2022. Hadron therapy achievements and challenges: the CNAO experience. Issue 1. In: Physics (Switzerland), vol. 4. MDPI, pp. 229–257. https://doi.org/10.3390/physics4010017.

Safai, S., Lin, S., Pedroni, E., 2004. Development of an inorganic scintillating mixture for proton beam verification dosimetry. Phys. Med. Biol. 49 (19), 4637–4655. https://doi.org/10.1088/0031-9155/49/19/013.

Sánchez-Doblado, F., Andreo, P., Capote, R., Leal, A., Perucha, M., Arráns, R., NúNú, L., Mainegra, E., Lagares, J.I., Carrasco, E., 2003. Ionization chamber dosimetry of small photon fields: a Monte Carlo study on stopping-power ratios for radiosurgery and IMRT beams. Med. Biol. Phys. Med. Biol. 48 (14), 2081–2099. https://doi.org/10.1088/0031-9155/48/14/304.

Santiago, M., Prokic, M., Molina, P., Marcazzó, J., Caselli, E., 2009. A tissue-equivalent radioluminescent fiberoptic probe for in-vivo dosimetry based on Mn-doped lithium tetraborate. IFMBE Proceed. 25 (3), 367–370. https://doi.org/10.1007/978-3-642-03902-7_104.

Santos, A.M.C., Depauw, N., 2020. Evaluating the use of silica and PMMA optical fibres as proton beam monitors. J. Phys. Conf. 1662 (1) https://doi.org/10.1088/1742-6596/1662/1/012029.

Santos, A.M.C., Gowda, R., Bezak, E., Afshar, V.S., 2019. Evaluation of a real-time optically stimulated luminescence beryllium oxide (BeO) fibre-coupled dosimetry system with a superficial 140 kVp X-ray beam. Physica Medica. Eur. J. Med. Plants 65, 167–171. https://doi.org/10.1016/j.ejmp.2019.08.021.

Savard, N., Potkins, D., Beaudry, J., Jirasek, A., Duzenli, C., Hoehr, C., 2018. Characteristics of a Ce-Doped silica fiber irradiated by 74 MeV protons. Radiat. Meas. 114, 19–24. https://doi.org/10.1016/j.radmeas.2018.03.010.

Schoepper, I., Dieterich, S., Trestrail, E.A., Kent, M.S., 2022. Pre-clinical and clinical evaluation of the HYPERSCINT plastic scintillation dosimetry research platform for *in vivo* dosimetry during radiotherapy. J. Appl. Clin. Med. Phys. 23 (4) https://doi.org/10.1002/acm2.13551.

Scott, A.J.D., Kumar, S., Nahum, A.E., Fenwick, J.D., 2012. Characterizing the influence of detector density on dosimeter response in non-equilibrium small photon fields. Phys. Med. Biol. 57 (14), 4461–4476. https://doi.org/10.1088/0031-9155/57/14/4461.

Shaharuddin, S., Hart, A., Cecchi, D.D., Bazalova-Carter, M., Foley, M., 2021. Real-time dosimetry of ultrahigh dose-rate x-ray beams using scintillation detectors. Proceed. IEEE Sens. https://doi.org/10.1109/SENSORS47087.2021.9639825, 2021-October.

Simiele, E.A., DeWerd, L.A., 2018. Characterization of spectral and intensity changes with measurement geometry in various light guides used in scintillation dosimetry. Med. Phys. 45 (7), 3417–3428. https://doi.org/10.1002/mp.12992.

Simiele, E., Kapsch, R.P., Ankerhold, U., Culberson, W., Dewerd, L., 2018. Spectral characterization of plastic scintillation detector response as a function of magnetic field strength. Phys. Med. Biol. 63 (8) https://doi.org/10.1088/1361-6560/aab56c.

Simiele, E., Viscariello, N., DeWerd, L., 2021. Monte Carlo modeling of the influence of strong magnetic fields on the stem-effect in plastic scintillation detectors used in radiotherapy dosimetry. Med. Phys. 48 (3), 1381–1394. https://doi.org/10.1002/mp.14637.

Son, J., Kim, M., Jeong, J., Lim, Y., Lee, S.B., Shin, D., Yoon, M., 2017. Characteristics of fiber-optic radiation sensor for passive scattering proton beams. J. Instrum. 12 (11), P11015 https://doi.org/10.1088/1748-0221/12/11/P11015.

Sosa, R.F., Alvarez, E.R., Camacho, M.A., Munoz, A.F., Rubio, J.O., 1995. Time-resolved spectroscopy of the Eu2+ luminescence in KCl:Ba2+, Eu2+ KCl:Sr2+, Eu2+ and KBr:Sr2+, Eu2+. J. Phys. Condens. Matter 7 (32), 6561. https://doi.org/10.1088/0953-8984/7/32/021.

Stefanowicz, S., Latzel, H., Lindvold, L.R., Andersen, C.E., Jäkel, O., Greilich, S., 2013. Dosimetry in clinical static magnetic fields using plastic scintillation detectors. Radiat. Meas. 56, 357–360. https://doi.org/10.1016/j.radmeas.2013.03.012.

Suchowerska, N., Jackson, M., Lambert, J., Yin, Y.B., Hruby, G., McKenzie, D.R., 2011. Clinical trials of a urethral dose measurement system in brachytherapy using scintillation detectors. Int. J. Radiat. Oncol. Biol. Phys. 79 (2), 609–615. https://doi.org/10.1016/j.ijrobp.2010.03.030.

Tanyi, J.A., Krafft, S.P., Ushino, T., Huston, A.L., Justus, B.L., 2010. Performance characteristics of a gated fiber-optic-coupled dosimeter in high-energy pulsed photon radiation dosimetry. Appl. Radiat. Isot. 68 (2), 364–369. https://doi.org/10.1016/j.apradiso.2009.10.042.

Tanyi, J.A., Nitzling, K.D., Lodwick, C.J., Huston, A.L., Justus, B.L., 2011. Characterization of a gated fiber-optic-coupled detector for application in clinical electron beam dosimetry. Med. Phys. 38 (2), 961–967. https://doi.org/10.1118/1.3539737.

Teichmann, T., Sommer, M., Henniger, J., 2013. Dose rate measurements with a ruby-based fiber optic radioluminescent probe. Radiat. Meas. 56, 347–350. https://doi.org/10.1016/j.radmeas.2013.03.027.

Teichmann, T., Sponner, J., Radtke, J., Henniger, J., 2017. Gated discrimination of the stem signal in pulsed radiation fields for a fiber optic dosimetry system based on the radioluminescence of beryllium oxide. Radiat. Meas. 106, 552–555. https://doi.org/10.1016/j.radmeas.2017.03.046.

Teichmann, T., Torres, M.J.G., Goethem, M. J. van, van der Graaf, E.R., Henniger, J., Jahn, A., Kiewiet, H.H., Sommer, M., Ullrich, W., Weinhold, C., Kormoll, T., 2018. Dose and dose rate measurements in proton beams using the luminescence of beryllium oxide. J. Instrum. 13 (10), P10015 https://doi.org/10.1088/1748-0221/13/10/P10015.

Teichmann, T., Torres, M.J.G., Makarevich, K., Polter, S., Lachmann, P., van der Graaf, E. R., Goethem, M. J. van, Jahn, A., Henniger, J., Zuber, K., Kormoll, T., 2019. Combined OSL-RL measurements for dosimetry in mixed LET proton fields. In: 2019 IEEE Nuclear Science Symposium and Medical Imaging Conference. NSS/MIC, pp. 1–3. https://doi.org/10.1109/NSS/MIC42101.2019.9059926.

Therriault-Proulx, F., Archambault, L., Beaulieu, L., Beddar, S., 2012. Development of a novel multi-point plastic scintillation detector with a single optical transmission line for radiation dose measurement. Phys. Med. Biol. 57 (21), 7147–7159. https://doi.org/10.1088/0031-9155/57/21/7147.

Therriault-Proulx, F., Beaulieu, L., Archambault, L., Beddar, S., 2013. On the nature of the light produced within PMMA optical light guides in scintillation fiber-optic dosimetry. Phys. Med. Biol. 58 (7), 2073–2084. https://doi.org/10.1088/0031-9155/58/7/2073.

Therriault-Proulx, F., Beddar, S., Briere, T.M., Archambault, L., Beaulieu, L., 2011. Technical note: removing the stem effect when performing Ir-192 HDR brachytherapy *in vivo* dosimetry using plastic scintillation detectors: a relevant and necessary step. Med. Phys. 38 (4), 2176–2179. https://doi.org/10.1118/1.3562902.

Therriault-Proulx, F., Wen, Z., Ibbott, G., Beddar, S., 2018. Effect of magnetic field strength on plastic scintillation detector response. Radiat. Meas. 116, 10–13. https://doi.org/10.1016/j.radmeas.2018.06.011.

Torrisi, L., 2000. Plastic scintillator investigations for relative dosimetry in proton-therapy. Nucl. Instrum. Methods Phys. Res. Sect. B Beam Interact. Mater. Atoms 170 (3), 523–530. https://doi.org/10.1016/S0168-583X(00)00237-8.

Traini, G., Mattei, I., Battistoni, G., Bisogni, M.G., De Simoni, M., Dong, Y., Embriaco, A., Fischetti, M., Magi, M., Mancini-Terracciano, C., Marafini, M., Mirabelli, R., Muraro, S., Patera, V., Schiavi, A., Sciubba, A., Solfaroli Camillocci, E., Valle, S.M., Sarti, A., 2019. Review and performance of the Dose Profiler, a particle therapy treatments online monitor. Phys. Med. 65, 84–93. https://doi.org/10.1016/j.ejmp.2019.07.010.

Uijtewaal, P., Côté, B., Foppen, T., de Vries, W., Woodings, S., Borman, P., Lambert-Girard, S., Therriault-Proulx, F., Raaymakers, B., Fast, M., 2023. Performance of the HYPERSCINT scintillation dosimetry research platform for the 1.5 T MR-linac. Phys. Med. Biol. 68 (4) https://doi.org/10.1088/1361-6560/acb30c.

Underwood, T.S.A., Rowland, B.C., Ferrand, R., Vieillevigne, L., 2015. Application of the Exradin W1 scintillator to determine Ediode 60017 and microDiamond 60019 correction factors for relative dosimetry within small MV and FFF fields. Phys. Med. Biol. 60 (17), 6669–6683. https://doi.org/10.1088/0031-9155/60/17/6669.

Vanreusel, V., Gasparini, A., Galante, F., Mariani, G., Pacitti, M., Cociorb, M., Giammanco, A., Reniers, B., Reulens, N., Shonde, T.B., Vallet, H., Vandenbroucke, D., Peeters, M., Leblans, P., Ma, B., Felici, G., Verellen, D., de Freitas Nascimento, L., 2022. Point scintillator dosimetry in ultra-high dose rate electron "FLASH" radiation therapy: a first characterization. Phys. Med. 103, 127–137. https://doi.org/10.1016/j.ejmp.2022.10.005.

Veronese, I., Cantone, M.C., Catalano, M., Chiodini, N., Fasoli, M., Mancosu, P., Mones, E., Moretti, F., Scorsetti, M., Vedda, A., 2013a. Study of the radioluminesence spectra of doped silica optical fibre dosimeters for stem effect removal. J. Phys. Appl. Phys. 46 (1) https://doi.org/10.1088/0022-3727/46/1/015101.

Veronese, I., Cantone, M.C., Chiodini, N., Coray, A., Fasoli, M., Lomax, A., Mones, E., Moretti, F., Vedda, A., 2010. Feasibility study for the use of cerium-doped silica fibres in proton therapy. Radiat. Meas. 45 (3–6) https://doi.org/10.1016/j.radmeas.2009.10.100.

Veronese, I., Cantone, M.C., Chiodini, N., Fasoli, M., Mones, E., Moretti, F., Vedda, A., 2013b. The influence of the stem effect in Eu-doped silica optical fibres. Radiat. Meas. 56, 316–319. https://doi.org/10.1016/j.radmeas.2013.01.043.

Veronese, I., Chiodini, N., Cialdi, S., D'Ippolito, E., Fasoli, M., Gallo, S., La Torre, S., Mones, E., Vedda, A., Loi, G., 2017. Real-time dosimetry with Yb-doped silica optical fibres. Phys. Med. Biol. 62 (10), 4218–4236. https://doi.org/10.1088/1361-6560/aa642f.

Veronese, I., De Mattia, C., Fasoli, M., Chiodini, N., Cantone, M.C., Moretti, F., Dujardin, C., Vedda, A., 2015. Role of optical fiber drawing in radioluminescence hysteresis of Yb-doped silica. J. Phys. Chem. C 119 (27). https://doi.org/10.1021/acs.jpcc.5b04987.

Veronese, I., Fasoli, M., Martini, M., Moretti, F., Vedda, A., Loi, G., Mones, E., 2007. Phosphorescence of SiO_2 optical fibres doped with Ce 3+ ions. Phys. Status Solidi (C) Curr. Top. Solid State Phys. 4 (3) https://doi.org/10.1002/pssc.200673758.

Veronese, I., Mattia, C. De, Fasoli, M., Chiodini, N., Mones, E., Cantone, M.C., Vedda, A., 2014. Infrared luminescence for real time ionizing radiation detection. Appl. Phys. Lett. 105 (6) https://doi.org/10.1063/1.4892880.

Wang, L.L.W., Beddar, S., 2011. Study of the response of plastic scintillation detectors in small-field 6 MV photon beams by Monte Carlo simulations. Med. Phys. 38 (3), 1596–1599. https://doi.org/10.1118/1.3554644.

Wang, L.L.W., Perles, L.A., Archambault, L., Sahoo, N., Mirkovic, D., Beddar, S., 2012. Determination of the quenching correction factors for plastic scintillation detectors in therapeutic high-energy proton beams. Phys. Med. Biol. 57 (23), 7767–7781. https://doi.org/10.1088/0031-9155/57/23/7767.

Watanabe, K., 2023. Applications of scintillators in optical-fiber-based detectors. Issue 1. In: Japanese Journal of Applied Physics, vol. 62. Institute of Physics. https://doi.org/10.35848/1347-4065/ac90a5.

Won Jang, K., Jae Yoo, W., Hun Shin, S., Shin, D., Lee, B., 2012. Fiber-optic Cerenkov Radiation Sensor for Proton Therapy Dosimetry.

Wootton, L., Holmes, C., Sahoo, N., Beddar, S., 2015. Passively scattered proton beam entrance dosimetry with a plastic scintillation detector. Phys. Med. Biol. 60 (3), 1185. https://doi.org/10.1088/0031-9155/60/3/1185.

Wootton, L., Kudchadker, R., Lee, A., Beddar, S., 2014. Real-time *in vivo* rectal wall dosimetry using plastic scintillation detectors for patients with prostate cancer. Phys. Med. Biol. 59 (3), 647–660. https://doi.org/10.1088/0031-9155/59/3/647.

Woulfe, P., Sullivan, F.J., O'Keeffe, S., 2016. Optical fibre sensors: their role in *in vivo* dosimetry for prostate cancer radiotherapy, 1. In: Cancer Nanotechnology, vol. 7. https://doi.org/10.1186/s12645-016-0020-y. Springer-Verlag Wien.

Yoo, W.J., Shin, S.H., Jeon, D., Hong, S., Kim, S.G., Sim, H.I., Jang, K.W., Cho, S., Lee, B., 2013. Simultaneous measurements of pure scintillation and Cerenkov signals in an integrated fiber-optic dosimeter for electron beam therapy dosimetry. Opt. Express 21 (23), 27770. https://doi.org/10.1364/oe.21.027770.

Yoon, J., Kim, J.I., Choi, C.H., Park, J.M., 2019. Characteristics of the Exradin W1 scintillator in the magnetic field. J. Appl. Clin. Med. Phys. 20 (9), 149–156. https://doi.org/10.1002/acm2.12707.

Yukihara, E.G., McKeever, S.W., 2008. Optically stimulated luminescence (OSL) dosimetry in medicine. Phys. Med. Biol. 53 (20) https://doi.org/10.1088/0031-9155/53/20/R01.

Zhang, J., Xiang, Y., Wang, C., Chen, Y., Tjin, S.C., Wei, L., 2022. Recent advances in optical fiber enabled radiation sensors. Issue 3. In: Sensors, vol. 22. https://doi.org/10.3390/s22031126. MDPI.